Published in final edited form as:

J Bone Miner Res. 2023 January ; 38(1): 70–85. doi:10.1002/jbmr.4732.

Conditional Loss of *Nmp4* in Mesenchymal Stem Progenitor Cells Enhances PTH-Induced Bone Formation

Emily G. Atkinson[1], **Michele Adaway**[1], **Daniel J. Horan**[1,2], **Crystal Korff**[3], **Angela Klunk**[1], **Ashley L. Orr**[1,5], **Katherine Ratz**[1,5], **Teresita Bellido**[6,7], **Lilian I. Plotkin**[1,4], **Alexander G. Robling**[1,2,4], **Joseph P. Bidwell**[1,4,¶]

[1]Department of Anatomy, Cell Biology, & Physiology, Indiana University School of Medicine (IUSM), Indianapolis, IN 46202

[2]Richard L. Roudebush Veterans Affairs Medical Center, Indianapolis, Indiana, USA.

[3]Department of Medical and Molecular Genetics, IUSM

[4]Indiana Center for Musculoskeletal Health, IUSM

[5]Present Address: Division of Biomedical Sciences, College of Osteopathic Medicine, Marian University Indianapolis, IN 46222

[6]Department of Physiology and Cell Biology University of Arkansas for Medical Sciences (UAMS), Little Rock, AR 72205

[7]Central Arkansas Veterans Healthcare System, Little Rock, AR 72205

Abstract

Activation of bone anabolic pathways is a fruitful approach for treating severe osteoporosis. Yet, FDA-approved osteoanabolics, e.g., parathyroid hormone (PTH), have limited efficacy. Improving their potency is a promising strategy for maximizing bone anabolic output. *Nmp4* (*Nuclear Matrix Protein 4*) global knockout mice, exhibit enhanced PTH-induced increases in trabecular bone but display no overt baseline skeletal phenotype. *Nmp4* is expressed in all tissues; therefore, to determine which cell type is responsible for driving the beneficial effects of *Nmp4* inhibition, we conditionally removed this gene from cells at distinct stages of osteogenic differentiation. *Nmp4-floxed* (*Nmp4*$^{fl/fl}$) mice were crossed with mice bearing one of three Cre drivers including (i) *Prx1Cre*+ to remove *Nmp4* from mesenchymal stem/progenitor cells (MSPCs) in long bones; (ii) *BglapCre*+ targeting mature osteoblasts and (iii) *Dmp1Cre*+ to disable *Nmp4* in osteocytes. Virgin female *Cre*+ and *Cre*− mice (10wks of age) were sorted into cohorts by weight and genotype. Mice were administered daily injections of either human PTH 1–34 at 30μg/kg, or vehicle for 4wks or 7wks. Skeletal response was assessed using dual-energy X-ray absorptiometry, microcomputed tomography, bone histomorphometry and serum analysis for remodeling markers. *Nmp4*$^{fl/fl}$*;Prx1Cre*+ mice virtually phenocopied the global *Nmp4*$^{-/-}$ skeleton in the femur, i.e., a mild baseline phenotype but significantly enhanced PTH-induced increase in femur trabecular bone volume/total volume (BV/TV) compared to their *Nmp4*$^{fl/fl}$*;Prx1Cre*− controls. This was

¶ Corresponding author: Joseph P Bidwell, jbidwell@iupui.edu, Department of Anatomy, Cell Biology & Physiology, Indiana University School of Medicine, Indianapolis IN, 46202.

DISCLOSURES: L.I.P. is a member of the FD/MAS Alliance Scientific Advisory Council

not observed in the spine, where *Prrx1* is not expressed. Heightened response to PTH was coincident with enhanced bone formation. Conditional loss of *Nmp4* from the mature osteoblasts (*Nmp4*$^{fl/fl}$;*BglapCre*+) failed to increase BV/TV or enhance PTH response. However, conditional disabling of *Nmp4* in osteocytes (*Nmp4*$^{fl/fl}$;*Dmp1Cre*+) increased BV/TV without boosting response to hormone under our experimental regimen. We conclude that *Nmp4*$^{-/-}$ Prx1-expressing MSPCs drive the improved response to PTH therapy, and that this gene has stage-specific effects on osteoanabolism.

Keywords

bone anabolism; osteoanabolics; osteoporosis; teriparatide

INTRODUCTION

Severe osteoporosis, the condition in which patients are plagued with painful bone fractures and the likelihood of acquiring more[1–3], is prevalent in the oldest old[4–8]. Osteoanabolics, drugs that add bone to the osteoporotic skeleton, are typically the initial therapy of choice for patients presenting with the severe form of the disease[9–11]. Current FDA-approved osteoanabolics, include the parathyroid hormone (PTH) analogue teriparatide [PTH 1–34], the parathyroid hormone related peptide analogue abaloparatide [PTHrp 1–34] and romosozumab, a sclerostin monoclonal antibody[12]. The latter is a monoclonal antibody that blocks the action of sclerostin, an antagonist of Wnt/βcatenin signaling, which is a central pathway driving bone anabolism[12–14]. Largely, these drugs enhance osteoanabolism by increasing osteoblast number and osteoblast secretory output[15,16]. These therapeutics enlarge the bone-forming osteoblast pool via a variety of mechanisms including the suppression of osteoblast apoptosis[17–19], activation of bone lining cells[20,21], and biasing mesenchymal stem/progenitor cell (MSPC) commitment to the osteogenic lineage instead of adipogenesis[18,19,22]. Furthermore, CD8+ T lymphocytes respond to intermittent PTH by producing Wnt10B, which promotes osteoblast activity and trabecular bone gains[23,24]. Romosozumab significantly increased osteoblast matrix output in experimental rats[25]. Lastly, romosozumab is a dual acting osteoporosis drug as it also represses the bone resorption arm of the remodeling process, perhaps by altering the osteoblast expression of cytokines that support osteoclastogenesis[16,26–28]. All these drugs are expensive[29,30] and the period in which they exert their maximum osteoanabolic effect is relatively short[31]. This is a drawback for treating a chronic degenerative disease and has motivated research on enhancing the potency of these therapeutics to maximize bone anabolic output.

We have previously reported that mice harboring a global loss-of-function mutation in the *Nmp4* gene (*Nuclear Matrix Protein 4*, a.k.a. *Zfp384*, *ZNF384*, *Ciz*) exhibit an enhanced PTH-induced bone formation response compared to their wild-type (WT) littermates without displaying an overt baseline skeletal phenotype[32–37]. Disabling *Nmp4* boosts the trabecular bone response to PTH without compromising the increase in the cortical compartment[32–37]. These mice are healthy under normal vivarium conditions and indeed are resistant to disease severity during influenza A viral infection and are less sensitive to high fat diet (HFD)-induced weight gain, increases in % fat mass, and decreases in

glucose tolerance and insulin sensitivity[38,39]. The *Nmp4* gene is a Cys_2His_2 zinc finger transcription factor expressed in all tissues[40]. Loss of *Nmp4* increases the number of bone marrow osteoprogenitors in experimental mice[34–36]. The isolated *Nmp4*$^{-/-}$ MSPCs mineralize more rapidly than WT cells and exhibit an enhanced capacity for glycolysis, the metabolic program that drives bone formation[35,37,41]. This trans-acting protein binds to over 15,000 DNA sites throughout the osteoblast genome and regulates the expression of over 5,000 genes in the osteoprogenitor and osteoblast transcriptomes[35,37]. In bone cells, Nmp4 appears to suppress protein production and delivery through governing ribosome biogenesis, translation, and the unfolded protein response (UPR)[37,42]. Secretory cells accommodate the synthesis, folding, and trafficking of proteins to ensure optimal export. Induction of the UPR activates a complex gene program that expands the processing capacity of the endoplasmic reticulum (ER)[42,43]. Remarkably, Nmp4 governs professional secretory cells in a tissue-specific manner. Whereas it suppresses osteoprogenitor/osteoblast secretion of bone matrix[37], it supports pancreatic beta cell insulin secretion[39] as well as lung epithelial cell production and release of the chemokines CCL2 and CXCL1 and bone marrow-derived macrophage release of CCL7[38].

Osteoprogenitors, osteoblasts, and osteocytes all are secretory cells controlling bone homeostasis and bone remodeling[44–46]. Discovering which cell type(s) drive the enhanced induced osteoanabolism in *Nmp4*$^{-/-}$ mice is crucial to understanding the limits of osteoanabolic pharmaceutical efficacy. To address this gap in knowledge we engineered a floxed loss-of function mouse model for *Nmp4* (*Nmp4*$^{fl/fl}$). We conditionally deleted *Nmp4* at different stages of the osteoblast-lineage differentiation. *Nmp4*$^{fl/fl}$ mice were crossed to one of three different bone-lineage Cre divers: *Prx1Cre*[47], which targets MSPCs in developing limb bud, *BglapCre*[48], which targets mature osteoblasts, and *Dmp1Cre*[49,50], which targets transitional osteocytes. The three conditional knockout models exhibited distinct bone phenotypes under our experimental regimen. The conditional loss of *Nmp4* from Prx1-expressing bone marrow MSPCs virtually phenocopied the global *Nmp4*$^{-/-}$ mouse response to PTH. Unexpectedly, our data revealed stage-specific roles for *Nmp4* in governing osteoanabolism.

MATERIALS AND METHODS

Mice:

The *Nmp4*$^{fl/fl}$ mouse was engineered using a vector from the European Conditional Mouse Mutagenesis Program (EUCOMM). The *Nmp4* (*Zfp384*) vector harbors a tm1a allele with conditional (tm1c) and knock-in reporter (tm1b) potential. The *loxP* sites flank exons 3–6, similar to our global knockout in which exons 4–7 were removed[32]. The LacZ/Neo cassette was deleted via Flp-mediated recombination of the Frt sites, which transforms the tm1a allele into the tm1c (conditional) allele. The vector was targeted in C57BL/6N ES cells and the *Nmp4*$^{fl/fl}$ mouse is on a pure C57BL/6N background. We deleted *Nmp4* at different stages of osteoblast-lineage differentiation by crossing the *Nmp4*$^{fl/fl}$ mice to one of three Cre drivers. To disable *Nmp4* in MSPCs we crossed the *Nmp4*$^{fl/fl}$ mice with *Prx1Cre* transgenic mice (*B6.Cg-Tg(Prxx1-cre)1Cjt/J*, stock no: 005584; The Jackson Laboratory, Bar Harbor, ME). To remove *Nmp4* from mature osteoblasts our floxed mice

were bred with *BglapCre* transgenic mice (*B6N.FVB-Tg(BGLAP-cre)Clem/J*, stock no: 019509; The Jackson Laboratory). *Nmp4* was deleted from transitional osteocytes by crossing the $Nmp4^{fl/fl}$ mice with the 8kb *Dmp1Cre* transgenic mouse[49,50]. To evaluate DNA recombination, we extracted bone and tail DNA from our mouse models for PCR analysis using the DNeasy Blood & Tissue Kits (Cat # 69504, Qiagen, Germantown, MD) following the manufacturer's instructions. The Indiana University Institutional Animal Care and Use Committee approved all engineering and breeding steps described in this investigation.

Osteocyte outgrowth cultures:

Primary osteocyte cultures were established using a standard protocol[51]. Briefly, osteocytes were isolated from long bones through extended collagenase digestions combined with EDTA-based decalcification. Small bone particles were placed in culture to yield an outgrowth of osteocyte-like cells. These cells were harvested in Pierce™ RIPA buffer (Thermo Scientific, Rockford, IL) and the lysates analyzed for total protein concentration using the Pierce™ BCA Protein Assay kit. These lysates were then evaluated for NMP4 protein (antibody, Sigma #HPA004051, Sigma Aldrich, St Louis, MO), PHEX protein (Anti-Phex/HYP antibody ab130629, Abcam, Waltham, MA) and β-actin protein (A5441, Sigma Aldrich) by Western analysis[42].

Treatment:

Virgin female mice were sorted into four cohorts by weight and genotype at 10wks of age. Typically, two to four mice were accommodated per cage under a 12:12-h light-dark regimen, and Labdiet Rodent 5001 diet and water was provided ad libitum. Mice were administered hPTH 1–34 acetate salt (Bachem Americas, Torrance, CA) at 30 μg/kg/day or vehicle for 4wks or 7wks. This dose of hormone is frequently used in rodents to evaluate PTH bone anabolic action[52,53]. The Indiana University Institutional Animal Care and Use Committee approved all experimental treatments described in this investigation.

Dual energy X-ray absorptiometry (DEXA):

Areal bone mineral density (aBMD, mg/cm^2) of the post-cranial skeleton, excluding the tail (whole body, WB), femur, spine (L3-L5), and tibia were evaluated in vivo using an X-ray PIXImus mouse densitometer (Piximus II; GE-Lunar Corp., Madison, WI) at the end of 4wks and 7wks treatments, as previously described[32,33].

Micro computed tomography (μCT):

Trabecular and cortical bone architectures were analyzed as we have previously described[35]. Briefly, left femurs and the L5 vertebra were dissected from experimental mice after euthanasia. The muscle and connective tissue were carefully removed from these bones and then transferred to 10% buffered formalin at 4°C for 48hr followed by transfer to 70% ethanol (4°C) until analyzed. After tissue preparation, the left femur and the L5 vertebral body were scanned using a Scanco μCT-35 (Scanco Medical AG, Brüttisellen CH). A 9.4mm of the distal femur was scanned and 2.6mm of the femur metaphysis was used in the trabecular and total bone analysis. The whole L5 vertebrae were scanned. Bones were

scanned at 10μm resolution, 55kV peak tube potential and 151ms integration time. Three-dimensional reconstructions using Scanco software provided the following parameters: trabecular bone volume/total volume (BV/TV), trabecular number (TbN; mm^{-1}), trabecular thickness (TbTh; mm), trabecular spacing (TbSp; mm), cortical thickness (mm), bone area (mm^2), total area (mm^2), marrow area (mm^2) and polar moment of inertia (pMOI; mm^4), maximum moment of inertia (Imax; mm^4), and minimum moment of inertia (Imin; mm^4).

Serum Biochemistry:

Activated serum osteocalcin, (Gla-osteocalcin) a marker for osteogenesis and remodeling, was measured using the Mouse Gla-Osteocalcin High Sensitive EIA Kit (TaKaRa, Shiga, Japan)[54]. Serum C-terminal telopeptides (CTX) was evaluated as an indicator for bone resorption using the RatLaps enzyme-linked immunosorbent assay (Immunodiagnostic System, Scottsdale, AZ)[36].

Immunohistochemistry:

All tissues were prepared at the Histology Core of the Indiana Center for Musculoskeletal Health. Formalin-fixed, paraffin-embedded sections of mouse bone marrow were evaluated for osterix with a primary antibody from Abcam (human anti-SP7/osterix; ab 94744; Cambridge, MA). These tissue sections were developed for analysis as previously described[35] using a modified protocol based on one reported by Nissenson and colleagues[55,56]. Small, round cells within the marrow exhibiting a brown nucleus indicating positive staining for osterix were counted as osteoprogenitors, and then the count normalized to the tissue area. Analysis was restricted within a 0.75- to 1-mm^2 area approximately 1 mm below the growth plate of the distal right femur. The stained bone marrow cells were counted using the OsteoMeasure High Resolution Digital Video System (OsteoMetrics, Decatur, GA).

Trabecular dynamic bone histomorphometry:

All tissues were prepared at the Histology Core of the Indiana Center for Musculoskeletal Health. These parameters were obtained as we have previously reported[33]. We analyzed the mice treated with PTH or vehicle for 4wks as opposed to 7wks since our earlier study with global *Nmp4*$^{-/-}$ mice indicated that changes in bone formation rate likely occur earlier in treatment, which is consistent with the observed precocious mineralization observed in vitro[33,35,37]. Briefly, mice were administered intraperitoneal injections of calcein green (20 mg/kg; Sigma-Aldrich) and alizarin red (25 mg/kg; Sigma-Aldrich) 6 and 3 days before euthanasia, respectively. Femurs were removed from experimental mice and fixed with 10% buffered formalin followed by transfer to 70% ethanol as described above. The anterior face of the epiphyseal plate of the right femur was cut to expose the marrow cavity. Methyl-methacrylate was used to embed the bones after dehydration with graded alcohols. Specimens were sectioned (4μm) using a Leica RM2255 microtome (Leica Microsystems, Buffalo Grove, IL). Tissue sections were then mounted unstained on microscope slides and scored using the OsteoMeasure High Resolution Digital Video System (OsteoMetrics, Decatur, GA) microscope system. The dynamic bone histomorphometry parameters of mineral apposition rate (MAR, μm/day), bone formation rate (BFR/BS, $\mu m^3/\mu m^2$/day), and mineralizing surface/bone surface (MS/BS, %) were obtained from a 0.75- to 1-mm^2

metaphyseal region of interest approximately 200–400μm from the distal femur growth plate.

Statistics:

JMP version 16 (SAS Institute, Cary, NC) was used to perform statistical analysis. A two-way ANOVA was employed to determine whether genotype or treatment influenced the parameter of interest and to evaluate whether an interaction occurred between the main effects. When an interaction between main effects was observed, all pairwise post hoc comparisons were performed to identify intergroup differences with p values ≤ 0.05 using a Tukey's HSD. We used a repeated-measures multivariate analysis of variance (MANOVA) to assess whether genotype or treatment had a significant impact on serum markers for bone formation or resorption during the experimental period (7wks), as well as to determine whether an interaction occurred between these main effects. Briefly, for all our analyses a significant genotype × treatment interaction indicated that the WT and the *Nmp4* conditional knockout mice responded differently to PTH under the described experimental regimen when comparing the four cohorts of WT-vehicle, WT-PTH, $Nmp4^{-/-}$ conditional knockout-vehicle, $Nmp4^{-/-}$ conditional knockout-PTH. Data is typically displayed using violin plots with staggered data points, showing the median and the quartiles. The sera data are linear graphs with each time point representing the average ± S.D.

RESULTS

Confirmation of Nmp4 conditional knockout mouse models:

A schematic representation of the cell target for each of our *Nmp4* conditional knockout models is shown in Supplemental Figure S1A. The $Nmp4^{fl/fl}$ mouse was engineered using a vector in which the *loxP* sites flank exons 3–6 (Supplemental Figure S1B), very similar to our *Nmp4* global knockout mice in which the *loxP* sites flank exons 4–7[32]. The $Nmp4^{fl/fl}$ mice were crossed over several generations with one of three Cre drivers, *Prx1Cre*, *BglapCre*, and *Dmp1Cre* (Supplemental Figure S1B), to achieve homozygosity for the *Nmp4* floxed allele with (+) or without (–) presence of the Cre transgene. We extracted DNA from femur, spine, and tail of our three conditional knockout models and their Cre− controls as described in Materials and Methods. PCR analysis confirmed DNA homologous recombination in the long bone of the $Nmp4^{fl/fl}$;*Prx1Cre*+ mice but no recombination in the $Nmp4^{fl/fl}$;*Prx1Cre*− controls (Supplemental Figure S1C). The DNA from the spine of the $Nmp4^{fl/fl}$;*Prx1Cre*+ and $Nmp4^{fl/fl}$;*Prx1Cre*− mice exhibited no DNA homologous recombination (Supplemental Figure S1C), consistent with previous observations that *Prrx1* is not expressed in the vertebral MSPCs[47]. This serves as an internal control for evaluating the influence of disabling *Nmp4* in limb MSPCs. The $Nmp4^{fl/fl}$;*BglapCre*+ and $Nmp4^{fl/fl}$;*Dmp1Cre*+ mice both exhibited DNA homologous recombination in long bones and spine, but no recombination in their Cre− controls (Supplemental Figure S1C). Additionally, we performed osteocyte outgrowth cultures to assess NMP4 protein expression in the conditional knockout models and their Cre− controls (Supplemental Figure S1D). Although these are not pure populations the osteocyte-enriched cultures derived from the *Cre*+ bones all showed a reduction in NMP4 protein expression compared to cells obtained from the Cre− bones. These data confirmed the validity of our conditional knockout models.

Conditional loss of Nmp4 from MSPCs amplifies the skeleton's response to PTH:

We employed μCT to evaluate bone architecture in the distal femur and spine (L5) from the *Nmp4*$^{fl/fl}$*;Prx1Cre*+ and *Nmp4*$^{fl/fl}$*;Prx1Cre*− mice as described in the Materials and Methods. The μCT reconstructions of the distal femurs obtained after 4wks and 7wks of treatment are shown in Figure 1A. These images are from mice that represent the median values from each of the four treatment cohorts, (i) *Nmp4*$^{fl/fl}$*;Prx1Cre*− VEH, (ii) *Nmp4*$^{fl/fl}$*;Prx1Cre*− PTH, (iii) *Nmp4*$^{fl/fl}$*;Prx1Cre*+ VEH, and (iv) *Nmp4*$^{fl/fl}$*;Prx1Cre*+ PTH. Visually, the *Nmp4*$^{fl/fl}$*;Prx1Cre*+ PTH cohort appeared to have the most femoral trabecular bone at both 4wks and 7wks of treatment (Figure 1A). A 2-way ANOVA with treatment and genotype as independent variables was used to analyze the distal femur trabecular BV/TV data. In this analysis to determine if PTH altered BV/TV the 2-way ANOVA compared hormone-treated mice with vehicle-treated, regardless of genotype. This assessment indicated a strong treatment effect at both 4wks and 7wks ($p<0.0001$). A post hoc Student's t-test showed that, as expected, PTH significantly increased the amount of femoral trabecular bone at this site (Supplmental Table S1). Similarly, to determine if loss of *Nmp4* in MSPCs altered BV/TV, the 2-way ANOVA combined all *Nmp4*$^{fl/fl}$*;Prx1Cre*+ mice to compare with all *Nmp4*$^{fl/fl}$*;Prx1Cre*− mice, regardless of treatment. There was a strong genotype effect under both 4wks and 7wks regimens ($p \leq 0.0001$, Figure 1B, Supplmental Table S1) and the post hoc Student's t-test indicated that the Cre+ mice, exhibited greater femoral BV/TV than the Cre− mice. The femur data also revealed a genotype x treatment interaction ($p=0.0369$ 4wks and $p<0.0001$ 7wks, Figure 1B) indicating that conditional loss of *Nmp4* in the long bone MSPCs enhances femoral response to osteoanabolic PTH. A post-hoc Tukey's HSD test was performed to investigate differences between the four test cohorts and showed that there was no difference in femoral BV/TV between the *Nmp4*$^{fl/fl}$*;Prx1Cre*+ VEH-treated and *Nmp4*$^{fl/fl}$*;Prx1Cre*− VEH-treated cohorts (Figure 1B, Supplmental Table S1). However, this analysis showed that the *Nmp4*$^{fl/fl}$*;Prx1Cre*+ PTH-treated mice had significantly greater trabecular BV/TV than the *Nmp4*$^{fl/fl}$*;Prx1Cre*− PTH-treated mice (Figure 1B, Supplmental Table S1). This is the skeletal response to PTH we have consistently observed with the *Nmp4* global knockout mice, i.e., the baseline skeletal phenotype is not different between the knockout and WT mice, the phenotype is only unmasked in response to an anabolic stimulus[32–37].

The L5 vertebral data showed a strong PTH treatment effect at 4wks and 7wks ($p<0.0001$) but as expected no genotype or genotype x treatment interaction (Figure 1C).

Conditional loss of *Nmp4* from MSPCs increased femoral trabecular number (TbN), increased femoral trabecular thickness (TbTh), and decreased femoral trabecular spacing (TbSp) at both 4wks and 7wks of treatment (Figures 2A–2F). There were strong genotype and treatment effects for all three parameters. The PTH-induced change in TbTh exhibited a genotype x treatment interaction at both 4wks and 7wks treatment (Figures 2B and 2E). The post hoc Tukey's HSD analysis revealed that the *Nmp4*$^{fl/fl}$*;Prx1Cre*+ PTH-treated mice had a significantly enhanced TbTh compared to the other three groups (Figure 2B and 2E, Supplmental Table S1).

We analyzed trabecular dynamic bone histomorphometry (Figure 3A) at 14wks of age/ 4wks of treatment, because our previous studies with global *Nmp4*$^{-/-}$ and *Nmp4*$^{+/+}$

WT mice showed no enhanced bone remodeling in the *null* mice at 17wks-20wks of age, despite showing increased femoral BV/TV compared to the WT mice[33,35]. Indeed, *Nmp4*$^{fl/fl}$*;Prx1Cre*+ mice showed a greater BFR/BS (genotype p=0.0112, Figure 3B) and MS/BS (genotype p=0.0176, Figure 3C) than their *Nmp4*$^{fl/fl}$*;Prx1Cre*− littermates at 14wks of age/4wks of treatment. Although there were strong treatment effects for these parameters, i.e., PTH significantly increased BFR/BS and MS/BS, neither showed a genotype x treatment interaction (Figure 3B and 3C). Finally, there was no changes in MAR in any cohorts (Figure 3D). These data suggest that the increase in bone formation is due to the increase in the number of active remodeling sites and not necessarily an increase in the vigor of individual osteoblasts at this particular time point[57].

PTH treatment of global *Nmp4*$^{-/-}$ mice boosts the increase in trabecular bone without blunting the increase in the cortical compartment[32–37], therefore we evaluated postcranial whole body (WB) aBMD, a parameter which is largely driven by cortical bone mass[58], using DEXA as described in the Materials and Methods. Our 2-way ANOVA assessment of the DEXA data revealed that PTH increased WB aBMD for the 4wks and 7wks regimens as expected (p<0.0001) (Figures 4A and 4B). There was a near significant genotype effect at 4wks (p=0.0792) and a significant effect (p=0.0407) at 7wks of treatment (Figures 4A and 4B). The post hoc Student's t-test showed that the *Nmp4*$^{fl/fl}$*;Prx1Cre*+ mice, i.e., those harboring *Nmp4*$^{-/-}$ MSPCs had a significantly higher WB aBMD than the *Nmp4*$^{fl/fl}$*;Prx1Cre*− controls when comparing across the four *Nmp4*$^{fl/fl}$*;Prx1Cre* treatment cohorts (Figure 4B, Supplmental Table S1). Similarly, the *Nmp4*$^{fl/fl}$*;Prx1Cre*+ mice exhibited significantly greater tibial aBMD (p=0.0013) and a near significant increase in femur aBMD (p=0.0621) (Table 1). However, spine (L3-L5) aBMD did not significantly differ from the *Nmp4*$^{fl/fl}$*;Prx1Cre*− mice (Table 1). These data are similar to the DEXA profiles we obtained from the global *Nmp4*$^{-/-}$ mice[32]. Additionally, we used μCT to assess the midshaft femoral cortical architecture at 7wks of treatment (Table 1). Our 2-way ANOVA assessment of these data revealed that PTH significantly increased total area, bone area, cortical thickness, pMOI, Imax, and Imin in both genotypes (Table 1). There was a nearly significant genotype effect for bone area and cortical thickness revealing that these parameters trended higher in the *Nmp4*$^{fl/fl}$*;Prx1Cre*+ mice. Consistent with these results the Imin, an index of mechanical resistance to bending, was significantly higher in the *Nmp4*$^{fl/fl}$*;Prx1Cre*+ mice compared to the *Nmp4*$^{fl/fl}$*;Prx1Cre*− controls (p=0.0114, Table 1). The midshaft femoral cortical architecture of the *Nmp4*$^{fl/fl}$*;Prx1Cre*+ mice was somewhat similar to that we previously described for the global *Nmp4*$^{-/-}$ mice[37]. Therefore, we conclude that conditional loss of *Nmp4* in MSPCs closely phenocopies the PTH-induced changes in skeletal architecture of the global *Nmp4*$^{-/-}$ mice.

Analyses of serum for bone formation and resorption markers were consistent with the enhanced osteoanabolic phenotype. Serum samples were obtained from each mouse at 0wks (baseline), 3wks, and 7wks (end of therapy). The *Nmp4*$^{fl/fl}$*;Prx1Cre*+ mice showed a significantly higher serum osteocalcin level as compared to the *Nmp4*$^{fl/fl}$*;Prx1Cre*− control mice using a repeated-measures MANOVA to analyze the ELISA dataset (genotype p=0.0444, Figure 5A). This bone formation marker peaked at 3wks of PTH therapy. We observed no significant change in serum CTX levels, a bone resorption marker, during the 7wks treatment period (Figure 5B). However, at the end of the 7wks therapy regimen mice

of both genotypes treated with PTH showed an upward trend in CTX. This elevated serum osteocalcin and small change in serum CTX is similar to that observed previously in the global *Nmp4*$^{-/-}$ mice[36].

Osterix is one of several markers for the numerous osteoprogenitor populations in the adult mouse bone marrow; these cells also form networks of perivascular and reticular cells as well as committing to chondrocytes and adipocytes[59–62]. Intermittent PTH recruits' cells from this population as a source of bone-forming osteoblasts[63]. Therefore, we assessed the osterix+ cell frequency approximately 1 mm below the growth plate of the distal right femur from mice after 7wks of therapy (Figure 6A, Supplemental Figure S2). PTH treatment significantly lowered the number of these cells/mm^2 in both the *Nmp4*$^{fl/fl}$*;Prx1Cre*+ and *Nmp4*$^{fl/fl}$*;Prx1Cre*− mice (treatment p=0.0030) (Figure 6A). This is consistent with the observed decrease in serum osteocalcin at 7wks, i.e., the decline of the PTH 'anabolic window'. Interestingly, the *Nmp4*$^{fl/fl}$*;Prx1Cre*+ mice harbored significantly fewer osterix+ cells at this time point than the *Nmp4*$^{fl/fl}$*;Prx1Cre*− littermates (genotype p=0.0028, Figure 6A, Supplmental Table S1). This suggests that loss of *Nmp4* in Prx1-/osterix-expressing MSPCs enhances their differentiation into osteoblasts during bone formation thus leaving the osteoprogenitor pool. It is also consistent with our previous observation that *Nmp4*$^{-/-}$ MSPCs exhibit a significantly accelerated mineralization in culture[35,37]. Indeed, PTH treatment equally increased the number of osterix-positive cells lining the bone surface in both genotypes at this late time point in treatment (Figure 6B, Supplemental Table S1).

Conditional loss of Nmp4 from osteocalcin-expressing osteoblasts did not result in heightened response to PTH:

We performed the identical PTH/VEH experiments with the *Nmp4*$^{fl/fl}$*;BglapCre* mouse model. In this model *Nmp4* is disabled once the bone cell differentiates into a mature osteocalcin-expressing osteoblast. A 2-way ANOVA with treatment and genotype as independent variables was used to evaluate the distal femur and L5 vertebra trabecular BV/TV data from this model (Figures 7A – 7D). As observed with the *Nmp4*$^{fl/fl}$*;Prx1Cre* mice, both 4wks and 7wks hormone treatment increased distal femur and L5 BV/TV in the *Nmp4*$^{fl/fl}$*;BglapCre* cohorts, i.e., the 2W ANOVA indicated strong treatment effects (p<0.0001, Figure 7A – 7D, Supplemental Table S1). However, unlike the *Nmp4*$^{fl/fl}$*;Prx1Cre*+ mice, conditional deletion of *Nmp4* using the *BglapCre* failed to augment trabecular BV/TV or to boost the response to PTH in the femur or L5 vertebra, i.e., there were no genotype effects or genotype x treatment interactions at 4wks or 7wks challenge (Figures 7A – 7D, Supplemental Table S1). Similarly, there were no genotype effects or genotype x treatment interactions at 7wks PTH challenge for TbN, TbTh, or TbSp (Table 2).

We assessed postcranial WB, femur, tibia, and spine (L3-L5) aBMD by DEXA and femoral cortical geometry using μCT in the *Nmp4*$^{fl/fl}$*;BglapCre* mice (Table 2). Treatment with PTH significantly increased aBMD in all sites, but there was no genotype effect after 7wks of treatment as observed with the *Nmp4*$^{fl/fl}$*;Prx1Cre*+ mice (Table 2). PTH significantly increased total area, bone area, cortical thickness, pMOI, Imax, and Imin in both *Nmp4*$^{fl/fl}$*;BglapCre*+ and *Nmp4*$^{fl/fl}$*;BglapCre*− mice (Table 2). Also, these conditional

knockout mice exhibited a modest but significant larger marrow area and lower cortical thickness (genotype effect $p<0.05$, Table 2). Finally, pMOI, a measurement of geometric resistance to torsion, was slightly but significantly higher in the *Nmp4*$^{fl/fl}$*;BglapCre*+ mice (Table 2). Therefore, we conclude that conditional loss of *Nmp4* in osteocalcin-expressing osteoblasts does not alter skeletal response to PTH and has only minor effects on bone structural phenotype. We therefore decided to forego further detailed analysis of this phenotype.

Conditional loss of Nmp4 from osteocytes has significant impact on skeletal architecture but does not alter the response to PTH:

Interestingly, conditional loss of *Nmp4* in osteocytes (*Nmp4*$^{fl/fl}$*;Dmp1Cre*+) gave rise to a unique skeletal phenotype. As with the other two conditional knockout models PTH significantly increased distal femur and L5 BV/TV at both 4wks and 7wks treatment, that is, there was a strong treatment effect (treatment $p<0.0001$, Figures 8A–8D). But in contrast to the *Nmp4*$^{fl/fl}$*;BglapCre*+ mice, the *Nmp4*$^{fl/fl}$*;Dmp1Cre*+ cohorts showed higher femoral BV/TV and L5 BV/TV compared to their *Nmp4*$^{fl/fl}$*;Dmp1Cre*− littermates at 7wks of treatment, namely, there was a strong genotype effect (femur genotype $p=0.0028$, Figure 8C; L5 genotype $p=0.0001$ Figure 8D, Supplemental Table S1). Intriguingly, these mice did not show a heightened response to PTH, i.e., there were no genotype x treatment interactions for either the femur or for L5 (Figures 8C and 8D, Supplemental Table S1).

Both the *Nmp4*$^{fl/fl}$*;Dmp1Cre*+ and *Nmp4*$^{fl/fl}$*;Dmp1Cre*− mice exhibited a PTH-induced increase in femoral trabecular number (TbN), increased femoral trabecular thickness (TbTh), and decreased femoral trabecular spacing (TbSp) at 4wks (treatment effect $p<0.05$, Figures 9A–9C, Supplemental Table S1). Similar changes were observed at 7wks of treatment except for the lack of change in TbTh (Figures 9D–9F). There were strong genotype effects for TbN ($p=0.0014$) and TbSp ($p=0.0013$) at 7wks treatment indicating that the *Nmp4*$^{fl/fl}$*;Dmp1Cre*+ mice exhibited a higher trabecular number with less space between them than their *Nmp4*$^{fl/fl}$*;Dmp1Cre*− littermates (Figures 9D and 9F, Supplemental Table S1). There were no genotype x treatment interactions for any of these parameters (Figures 9A–9F, Supplemental Table S1).

As with the *Nmp4*$^{fl/fl}$*;Prx1Cre* mice we analyzed trabecular dynamic bone histomorphometry during the first 4wks of therapy for the *Nmp4*$^{fl/fl}$*Dmp1Cre* cohorts. There was an upward trend for both BFR/BS and MS/BS in the *Nmp4*$^{fl/fl}$*;Dmp1Cre*+ mice but this was not statistically significant (Table 3). These data are consistent with our μCT results showing no enhancement of femur or L5 vertebra BV/TV at the 4wks time point but at the 7wks time point.

We assessed aBMD for postcranial WB, femur, tibia, and spine (L3-L5) of the *Nmp4*$^{fl/fl}$*;Dmp1Cre* mice using DEXA (Table 3). Our 2-way ANOVA evaluation of these data revealed that PTH significantly increased aBMD for all these skeletal parameters at 7wks (treatment $p<0.0001$) but there were no genotype effects or genotype x treatment interactions (Table 3). Evaluation of the femoral cortical geometry using μCT revealed that PTH significantly increased midshaft total area, bone area, cortical thickness, marrow area, pMOI, Imax, and Imin in both genotypes but there was no genotype effects or genotype x

treatment interactions for any of these parameters (Table 3). We conclude that conditional loss of *Nmp4* in osteocytes alters the trabecular architecture in long bone and spine but does not modify the skeleton's response to hormone and that *Nmp4* control of osteoanabolism is dependent upon the stage of osteogenic differentiation.

The *Nmp4*$^{fl/fl}$*;Dmp1Cre*+ mice exhibited a significantly enhanced hormone-induced increase in serum osteocalcin as compared to the *Nmp4*$^{fl/fl}$*;Dmp1Cre*− mice (Figure 10A). Serum osteocalcin showed a profile very similar to that observed for the *Nmp4*$^{fl/fl}$*;Prx1Cre* mice. PTH induced a peak in this marker at 3wks of therapy, which had decreased by 7wks (Figure 10A). There were strong genotype ($p=0.0397$) and treatment ($p<0.0001$) effects as well as a genotype x treatment interaction ($p=0.0073$). Serum CTX exhibited a rise with PTH treatment in both *Nmp4*$^{fl/fl}$*;Dmp1Cre*+ and *Nmp4*$^{fl/fl}$*;Dmp1Cre*− mice, but there were no significant differences between the genotypes (Figure 10B).

PTH treatment significantly decreased the osterix+ cell frequency 1mm below the femoral growth plate in both the *Nmp4*$^{fl/fl}$*;Dmpr1Cre*+ and *Nmp4*$^{fl/fl}$*;Dmp1Cre*− mice after 7wks of therapy (treatment, $p=0.0240$, Table 3, Supplemental Figure S2). However, there was no difference in osterix+ cell frequency between the *Cre*+ and *Cre*− phenotypes. This was different from the observed difference in osterix+ cell numbers between the *Nmp4*$^{fl/fl}$*;Prx1Cre*+ and *Nmp4*$^{fl/fl}$*;Prx1Cre*− mice (Figure 6). This is consistent with our hypothesis that loss of *Nmp4* in Prx1-/osterix-expressing MSPCs accelerates their differentiation into osteoblasts during bone formation. The *Nmp4*$^{fl/fl}$*;Dmp1Cre*+ mice harbor osteoprogenitors that express *Nmp4* thus do not show an accelerated differentiation[35,37]. As observed with the *Nmp4*$^{fl/fl}$*;Prx1Cre* mice, PTH treatment equally increased the number of osterix-positive cells lining the bone surface in both *Nmp4*$^{fl/fl}$*;Dmp1Cre*+ and Cre− genotypes (Table 3).

DISCUSSION:

We have previously reported that global *Nmp4*$^{-/-}$ mice are healthy and have no patent baseline phenotype but exhibit an exaggerated bone formation response to the osteoanabolic PTH (1–34)[32–37]. *Nmp4* is expressed in all tissues[40], therefore to determine which cell type is responsible for driving the beneficial effects of *Nmp4* inhibition, we engineered three conditional knockout models removing this gene at three stages of bone cell development including long bone MSPCs (*Nmp4*$^{fl/fl}$*;Prx1Cre*), mature, osteocalcin-expressing osteoblasts (*Nmp4*$^{fl/fl}$*;BglapCre*), and transitional osteocytes (*Nmp4*$^{fl/fl}$*;Dmp1Cre*).

The present data show that mice harboring conditional deletion of *Nmp4* from Prx1-expressing MSPCs virtually phenocopy the global *Nmp4*$^{-/-}$ skeleton[32–37]. The non-inducible *Prx1Cre* is active at the limb bud stage (E 9.5) and will disable the target gene in all cells of mesenchymal origin in the limb, including stromal cells, osteoblasts, osteocytes, chondrocytes, and adipocytes[47]. Like the global *Nmp4*$^{-/-}$ mice, the *Nmp4*$^{fl/fl}$*;Prx1Cre*+ mice showed a significantly enhanced PTH-induced increase in femur BV/TV and TbTh compared to their *Nmp4*$^{fl/fl}$*;Prx1Cre*− cohorts. These conditional knockout mice also exhibited increased femoral TbN and decreased TbSp consistent with improved bone architecture. As with the global *null* mice, challenge with PTH was necessary to fully

unmask the enhanced femoral BV/TV and no differences in this skeletal parameter was observed between the *Cre*+ and *Cre*− vehicle-treated groups. Additionally, this amplified response to PTH was lost in the L5 spine of the *Nmp4*$^{fl/fl}$*;Prx1Cre*+ mice where *Prrx1* is not expressed[47], thus acting as an internal control. Disabling *Nmp4* in MSPCs using the *Prx1Cre* driver significantly increased WB aBMD (a parameter which is largely driven by cortical bone mass)[58] and tibial aBMD compared to *Nmp4*$^{fl/fl}$*;Prx1Cre*− controls. Similarly, the *Nmp4*$^{fl/fl}$*;Prx1Cre*+ mice showed a nearly significant increase in femoral aBMD. These improvements in aBMD are very similar to the profile we reported for the global *Nmp4*$^{-/-}$ mice[32].

Consistent with the improved bone architecture of the *Nmp4*$^{fl/fl}$*;Prx1Cre*+ mice, was the elevated anabolic bone remodeling, i.e., heightened BFR/BS and MS/BS, coincident with the enhanced serum osteocalcin. Both *the Nmp4*$^{fl/fl}$*;Prx1Cre*+ and *Nmp4*$^{fl/fl}$*;Prx1Cre*− exhibited a significant PTH-induced decrease in bone marrow osteoprogenitors (osterix-positive cells) at the end of the 7wk treatment period when serum osteocalcin was declining. Additionally, the *Nmp4*$^{fl/fl}$*;Prx1Cre*+ harbored significantly fewer such cells than the Cre− controls. Intermittent PTH accelerates osteoprogenitor differentiation into osteoblasts[64] and our data suggest that loss of *Nmp4* in Prx1-expressing MSPCs further promotes this phenomenon. Indeed, isolated *Nmp4*$^{-/-}$ MSPCs exhibit an accelerated differentiation into mineralizing osteoblasts[35,37]. Additionally, in the present study, PTH treatment increased the number of osterix-positive cells lining the bone surface in both genotypes, consistent with osteoprogenitor recruitment into the differentiation pathway. We have previously reported that ovariectomized global *Nmp4*$^{-/-}$ mice harbor more osterix+ cells than their WT littermates after 8wks of PTH treatment from 16wks to 24wks of age[36]. This difference between global *Nmp4*$^{-/-}$ mice and the *Nmp4*$^{fl/fl}$*;Prx1Cre*+ mice is not yet clear. The global *Nmp4*$^{-/-}$ mice have a significant increase in bone marrow CD8+ T cells[34,35]. These cells play an important role in PTH-induced anabolic bone formation[23,24,65,66]. They express PTH receptors and upon hormone challenge release Wnt10B, a potent growth factor for osteoprogenitors[23,24,65,66]. Therefore, the *Nmp4*$^{-/-}$ CD8+T cells may be supporting the replenishment of the osterix+ cell pool in the PTH-treated global *null* mice, more so than the *Nmp4*$^{+/+}$ CD8+T cells in the conditional knockout animals.

The present data suggest that the *Nmp4*$^{-/-}$ skeletal phenotype is contingent on when the gene is turned off during osteoblast differentiation. Disabling this gene at the stage of the MSPC/osteoprogenitor in the *Nmp4*$^{fl/fl}$*;Prx1Cre*+ mice improved trabecular architecture and enhanced BV/TV response to PTH. However, inactivating *Nmp4* at the stage of the transitional osteocyte (*Nmp4*$^{fl/fl}$*;Dmp1Cre*+), improved trabecular architecture but not the response to PTH. Osteocytes regulate bone anabolism by the local release of factors that constrain (sclerostin, Dkk1) or increase (PGE_2, IGF-1, Wnts) osteoblast-mediated bone formation[67–72]. We propose that the *Nmp4*$^{-/-}$ osteocytes of both the *Nmp4*$^{fl/fl}$*;Prx1Cre*+ and *Nmp4*$^{fl/fl}$*;Dmp1Cre*+ mice release an amplified anabolic signal. This signal activates the hyper-responsive *Nmp4*$^{-/-}$ MSPCs/osteoblasts in the *Nmp4*$^{fl/fl}$*;Prx1Cre*+ mice and the less reactive or susceptive *Nmp4*$^{+/+}$ MSPCs/osteoblasts in the *Nmp4*$^{fl/fl}$*;Dmp1Cre*+ mice. This is consistent with our observation *Nmp4*$^{fl/fl}$*;Prx1Cre*+ mice harbor fewer osterix-expressing cells than their Cre− controls after 7wks perhaps due to an enhanced/accelerated differentiation into osteoblasts but no such difference between the *Nmp4*$^{fl/fl}$*;Dmp1Cre*+

mice and their Cre− controls was observed. The *Nmp4*$^{fl/fl}$*;Dmp1Cre*+ mice required 7wks before exhibiting a higher femoral and L5 BV/TV than their Cre− controls compared to only 4wks for the *Nmp4*$^{fl/fl}$*;Prx1Cre*+ mice to surpass their Cre− controls. Correspondingly, the *Nmp4*$^{fl/fl}$*;Prx1Cre*+ mice showed a strong genotype x treatment interaction for the PTH therapeutic increase in femoral BV/TV at both 4wks and 7wks but this parameter did not reach statistical significance in the *Nmp4*$^{fl/fl}$*;Dmp1Cre*+. Finally, the *Nmp4*$^{fl/fl}$*;Dmp1Cre*+ did not show an enhanced bone remodeling rate (BFR/BS and MS/BS) at 14wks of age/4wks treatment in contrast to the *Nmp4*$^{fl/fl}$*;Prx1Cre*+ mice.

Remarkably, conditional loss of *Nmp4* from the mature osteocalcin-expressing osteoblasts (*Nmp4*$^{fl/fl}$*;BglapCre*+) had no impact on trabecular architecture or PTH-induced increases in bone formation and only modest effects on some femoral cortical parameters. This was unexpected since *Nmp4*$^{-/-}$ MSPCs derived from our global *Nmp4*$^{-/-}$ mice differentiate into osteoblasts that display precocious mineralization and increased secretion of collagen[35,37]. One hypothesis is that *Nmp4* acts as a ‘scaling factor’ i.e., it controls allocation of the cell proteome supporting the establishment of distinct secretory floorplans for osteoblasts and again for osteocytes early in the sequential developmental stage-specific transitions into these unique cell types. Scaling factors are evolutionarily conserved transcription factors that early in differentiation, adjust expression of large subsets of genes necessary for supporting the requirements of professional secretory cells[73–78]. The timing of the action of these scaling factors within the differentiation program of the professional secretory cell is critical. MIST1 and CREB3L2 have been proposed as scaling factors in this context and the UPR transcription factor XBP1 has been shown to be a co-regulator with both these proteins in establishing the professional secretory cell phenotype[73–80]. MIST1, the master regulator of exocrine secretory cell architecture, targets hundreds of genes involved in protein synthesis, processing, transport, and exocytosis networks[80,81]. Similarly, CREB3L2 is a scaling factor for translation capacity in pituitary secretory cells and governs ~75% of regulatory and effector genes for translation[77]. Additionally, both MIST1 and CREB3L2 are involved in functional interactions with XBP1 to co-regulate several genes essential for mediating the proactive or “physiological UPR”[77,80,82]. Activation of this pathway protects the secretory cell from persistent massive protein synthesis and secretion by preventing the engagement of ER degradation and the pro-death apoptotic response[77,80,82–85]. The target transcriptome of *Nmp4* is very similar to these other scaling factors in that it influences the expression of hundreds of genes involved in ribosome biogenesis, translation, and the UPR[35,37,42]. Additionally, it has a significant impact on the activity of numerous secretory cells[38,39,86]. In our scaling factor hypothesis, *Nmp4* actually suppresses the allocation of the secretory cell proteome during the transition from MSPC to osteoblast, targeted by *Nmp4*$^{fl/fl}$*;Prx1Cre*+. Delaying the removal of *Nmp4* until the mature osteoblast stage (*Nmp4*$^{fl/fl}$*;BglapCre*+) may therefore be too late for having any influence on establishing the capacity of the osteoblast secretory floorplan, the primary bone-former. Furthermore, we propose that deleting *Nmp4* during the transitional period of osteocyte development (*Nmp4*$^{fl/fl}$*;Dmp1Cre*+) would be expected to affect the distinct secretory ultrastructure and function of the mature osteocyte[87–92].

Although intriguing, the scaling factor hypothesis is not fully supported by our present data. The dynamic bone histomorphometry analysis at 4wks treatment showed that *Nmp4*

deletion did not affect individual osteoblast activity, e.g., MAR. Rather, the changes in bone formation rate seem to be driven solely by increases in osteoblast coverage (e.g., MS/BS) at this point in therapy. A more detailed and comprehensive time course study is required. Additionally, this raises the question as to why the *Nmp4*$^{fl/fl}$*;BglapCre*+ mice do not ultimately give rise to a mouse that phenocopies the *Nmp4*$^{fl/fl}$*;Dmp1Cre*+ phenotype? It is not clear why *Nmp4*$^{fl/fl}$*;BglapCre*+-derived osteocytes are not equivalent to *Nmp4*$^{fl/fl}$*;Dmp1Cre*+ derived osteocytes, particularly when both show a decrease in NMP4 expression. If the scaling factor hypothesis is operative, then the skeletal phenotype will be exquisitely sensitive to the precise moment when *Nmp4* is inactivated during differentiation. Therefore, the striking differences between the *Nmp4*$^{fl/fl}$*;BglapCre*+ and *Nmp4*$^{fl/fl}$*;Dmp1Cre*+ mice may reflect the difference in time and space when *Bglap* and *Dmp1* become active as the cell progresses through its various developmental stages. Additionally, the mature osteoblast population is heterogeneous and not all these cells express *Bglap*[93–96]. Furthermore, not all mature osteoblasts, i.e., *Bglap*-expressing cells, give rise to osteocytes; some become bone lining cells, and some are lost to apoptosis[92,97,98]. Therefore, the architecture of the *Nmp4*$^{-/-}$ osteocyte lacunocanalicular network may differ between the *Nmp4*$^{fl/fl}$*;BglapCre*+ and *Nmp4*$^{fl/fl}$*;Dmp1Cre*+ mice. Further investigations are required to address whether the scaling factor hypothesis can account for any of the temporal/spatial cellular dynamics of the *Nmp4* anti-anabolic axis.

It is important to recognize the limitations of the present data, which provide the basis for future experimental approaches. Ultrastructural analysis of the osteoblast and osteocyte endoplasmic reticulum and Golgi apparatus is required to interrogate the impact of *Nmp4* on the secretory infrastructure of these cells[99,100]. The use of additional Cre-drivers, e.g., to remove *Nmp4* from adipocytes or chondrocytes will further parse the *Prx1Cre* results to determine whether the enhanced osteoanabolic phenotype is driven strictly by osteoblast lineage cells. There are several Cre-drivers that will allow a refinement of the apparent stage-specific effects of *Nmp4* on the skeletal phenotype including induced Cre-recombinase models to enable the control the *Nmp4* expression both spatially and temporally[101–104]. Expansion of the window for monitoring dynamic bone histomorphometry/histology coupled to lineage tracing will provide a more comprehensive analysis of how loss of *Nmp4* primes bone for the enhanced response to osteoanabolic therapy.

In summary, we used a genetic approach in mice to conditionally disrupt the transcription factor *Nmp4* in cells at different stages of the osteogenic lineage. Mice were subjected to intermittent PTH for 4wks or 7wks. Bone responses were assessed by DEXA, μCT, dynamic histomorphometry, bone histology, and serum analysis. Results showed that conditional loss of *Nmp4* in Prx1-expressing MSPCs significantly enhanced PTH-induced increases in trabecular bone, closely phenocopying previous outcomes obtained with global *Nmp4*$^{-/-}$ mice. Conditional deletion of *Nmp4* from mature osteoblasts had little impact on bone architecture and no effect on bone response to PTH, whereas deletion from transitional osteocytes increased trabecular architecture but not the response to intermittent hormone treatment. We conclude *Nmp4*$^{-/-}$ Prx1-expressing MSPCs drive the enhanced response to PTH and *Nmp4* control of osteoanabolism is dependent upon the stage of osteogenic differentiation.

Supplementary Material

Refer to Web version on PubMed Central for supplementary material.

ACKNOWLEDGEMENTS:

This work was supported by National Institutes of Health Grants 1R01 AR073739 to J.P.B. and R01 AR053237 to A.G.R.; VA grants I01 BX005861 and IK6 BX 003783 to A.G.R.; and support from T32 AR065971 to E.G.A and C.K, and Veterans Research Administration Merit Award 1I0 1BX005154 to L.I.P.

DATA AVAILABILITY STATEMENT:

The data that support the findings of this study are available from the corresponding author upon reasonable request.

REFERENCES

1. Catalano A, Martino G, Morabito N, Scarcella C, Gaudio A, Basile G, et al. Pain in Osteoporosis: From Pathophysiology to Therapeutic Approach. Drugs Aging. Oct 2017;34(10):755–65. Epub 2017/10/06. [PubMed: 28980156]
2. Huang CY, Liao LC, Tong KM, Lai HL, Chen WK, Chen CI, et al. Mediating effects on health-related quality of life in adults with osteoporosis: a structural equation modeling. Osteoporosis international : a journal established as result of cooperation between the European Foundation for Osteoporosis and the National Osteoporosis Foundation of the USA. Mar 2015;26(3):875–83. Epub 2014/12/06. [PubMed: 25477231]
3. International Osteoporosis Foundation. Diagnosing osteoporosis. 2017.
4. Strom O, Lauppe R, Ljunggren O, Spangeus A, Ortsater G, O'Kelly J, et al. Real-world effectiveness of osteoporosis treatment in the oldest old. Osteoporosis international : a journal established as result of cooperation between the European Foundation for Osteoporosis and the National Osteoporosis Foundation of the USA. Mar 30 2020. Epub 2020/04/02.
5. Cummings SR, Melton LJ. Epidemiology and outcomes of osteoporotic fractures. Lancet (London, England). May 18 2002;359(9319):1761–7. Epub 2002/06/07. [PubMed: 12049882]
6. Amin S, Achenbach SJ, Atkinson EJ, Khosla S, Melton LJ, 3rd. Trends in fracture incidence: a population-based study over 20 years. Journal of bone and mineral research : the official journal of the American Society for Bone and Mineral Research. Mar 2014;29(3):581–9. Epub 2013/08/21. [PubMed: 23959594]
7. Rizzoli R Postmenopausal osteoporosis: assessment and management. Best Practice & Research Clinical Endocrinology & Metabolism. 2018;32(5):739–57. [PubMed: 30449552]
8. Lippuner K, Johansson H, Kanis J, Rizzoli R. Remaining lifetime and absolute 10-year probabilities of osteoporotic fracture in Swiss men and women. Osteoporosis international. 2009;20(7):1131–40. [PubMed: 18974918]
9. Russell LA. Management of difficult osteoporosis. Best practice & research Clinical rheumatology. Dec 2018;32(6):835–47. Epub 2019/08/21. [PubMed: 31427058]
10. Kendler DL, Marin F, Zerbini CAF, Russo LA, Greenspan SL, Zikan V, et al. Effects of teriparatide and risedronate on new fractures in post-menopausal women with severe osteoporosis (VERO): a multicentre, double-blind, double-dummy, randomised controlled trial. Lancet (London, England). Jan 20 2018;391(10117):230–40. Epub 2017/11/14. [PubMed: 29129436]
11. Oswald AJ, Berg J, Milne G, Ralston SH. Teriparatide treatment of severe osteoporosis reduces the risk of vertebral fractures compared with standard care in routine clinical practice. Calcified tissue international. Feb 2014;94(2):176–82. Epub 2013/09/13. [PubMed: 24026567]
12. Anagnostis P, Gkekas NK, Potoupnis M, Kenanidis E, Tsiridis E, Goulis DG. New therapeutic targets for osteoporosis. Maturitas. Feb 2019;120:1–6. Epub 2018/12/26. [PubMed: 30583758]
13. Holdsworth G, Roberts SJ, Ke HZ. Novel actions of sclerostin on bone. Journal of molecular endocrinology. Feb 1 2019;62(2):R167–r85. Epub 2018/12/12. [PubMed: 30532996]

14. Delgado-Calle J, Sato AY, Bellido T. Role and mechanism of action of sclerostin in bone. Bone. Mar 2017;96:29–37. Epub 2016/10/25. [PubMed: 27742498]
15. Wein MN, Kronenberg HM. Regulation of Bone Remodeling by Parathyroid Hormone. Cold Spring Harbor perspectives in medicine. Aug 1 2018;8(8). Epub 2018/01/24.
16. Ke HZ, Roberts SJ, Holdsworth G. Pharmacologic basis of sclerostin inhibition. Principles of Bone Biology: Elsevier; 2020. p. 1711–31.
17. Jilka RL, Weinstein RS, Bellido T, Roberson P, Parfitt AM, Manolagas SC. Increased bone formation by prevention of osteoblast apoptosis with parathyroid hormone. The Journal of clinical investigation. Aug 1999;104(4):439–46. Epub 1999/08/17. [PubMed: 10449436]
18. Balani DH, Trinh S, Xu M, Kronenberg HM. Sclerostin Antibody Administration Increases the Numbers of Sox9creER+ Skeletal Precursors and Their Progeny. Journal of bone and mineral research : the official journal of the American Society for Bone and Mineral Research. Apr 2021;36(4):757–67. Epub 2021/01/06. [PubMed: 33400836]
19. Miao D, He B, Jiang Y, Kobayashi T, Sorocéanu MA, Zhao J, et al. Osteoblast-derived PTHrP is a potent endogenous bone anabolic agent that modifies the therapeutic efficacy of administered PTH 1–34. The Journal of clinical investigation. Sep 2005;115(9):2402–11. Epub 2005/09/03. [PubMed: 16138191]
20. Kim SW, Pajevic PD, Selig M, Barry KJ, Yang JY, Shin CS, et al. Intermittent parathyroid hormone administration converts quiescent lining cells to active osteoblasts. Journal of bone and mineral research : the official journal of the American Society for Bone and Mineral Research. Oct 2012;27(10):2075–84. Epub 2012/05/25. [PubMed: 22623172]
21. Kim SW, Lu Y, Williams EA, Lai F, Lee JY, Enishi T, et al. Sclerostin Antibody Administration Converts Bone Lining Cells Into Active Osteoblasts. Journal of bone and mineral research : the official journal of the American Society for Bone and Mineral Research. May 2017;32(5):892–901. Epub 2016/11/20. [PubMed: 27862326]
22. Fan Y, Hanai JI, Le PT, Bi R, Maridas D, DeMambro V, et al. Parathyroid Hormone Directs Bone Marrow Mesenchymal Cell Fate. Cell metabolism. Mar 7 2017;25(3):661–72. Epub 2017/02/07. [PubMed: 28162969]
23. Terauchi M, Li JY, Bedi B, Baek KH, Tawfeek H, Galley S, et al. T lymphocytes amplify the anabolic activity of parathyroid hormone through Wnt10b signaling. Cell metabolism. Sep 2009;10(3):229–40. Epub 2009/09/03. [PubMed: 19723499]
24. Pacifici R T cells, osteoblasts, and osteocytes: interacting lineages key for the bone anabolic and catabolic activities of parathyroid hormone. Annals of the New York Academy of Sciences. Jan 2016;1364:11–24. Epub 2015/12/15. [PubMed: 26662934]
25. Ominsky MS, Brown DL, Van G, Cordover D, Pacheco E, Frazier E, et al. Differential temporal effects of sclerostin antibody and parathyroid hormone on cancellous and cortical bone and quantitative differences in effects on the osteoblast lineage in young intact rats. Bone. Dec 2015;81:380–91. Epub 2015/08/12. [PubMed: 26261096]
26. Cosman F, Crittenden DB, Adachi JD, Binkley N, Czerwinski E, Ferrari S, et al. Romosozumab Treatment in Postmenopausal Women with Osteoporosis. The New England journal of medicine. Oct 20 2016;375(16):1532–43. Epub 2016/11/01. [PubMed: 27641143]
27. Lewiecki EM, Blicharski T, Goemaere S, Lippuner K, Meisner PD, Miller PD, et al. A Phase III Randomized Placebo-Controlled Trial to Evaluate Efficacy and Safety of Romosozumab in Men With Osteoporosis. The Journal of clinical endocrinology and metabolism. Sep 1 2018;103(9):3183–93. Epub 2018/06/23. [PubMed: 29931216]
28. Saag KG, Petersen J, Brandi ML, Karaplis AC, Lorentzon M, Thomas T, et al. Romosozumab or Alendronate for Fracture Prevention in Women with Osteoporosis. The New England journal of medicine. Oct 12 2017;377(15):1417–27. Epub 2017/09/12. [PubMed: 28892457]
29. Strom O, Borgstrom F, Kanis JA, Compston J, Cooper C, McCloskey EV, et al. Osteoporosis: burden, health care provision and opportunities in the EU: a report prepared in collaboration with the International Osteoporosis Foundation (IOF) and the European Federation of Pharmaceutical Industry Associations (EFPIA). Arch Osteoporos. 2011;6:59–155. Epub 2012/08/14. [PubMed: 22886101]

30. Conley RB, Adib G, Adler RA, Åkesson KE, Alexander IM, Amenta KC, et al. Secondary Fracture Prevention: Consensus Clinical Recommendations from a Multistakeholder Coalition. Journal of bone and mineral research : the official journal of the American Society for Bone and Mineral Research. Jan 2020;35(1):36–52. Epub 2019/09/21. [PubMed: 31538675]
31. Tabacco G, Bilezikian JP. Osteoanabolic and dual action drugs. Br J Clin Pharmacol. Jun 2019;85(6):1084–94. Epub 2018/09/16. [PubMed: 30218587]
32. Robling AG, Childress P, Yu J, Cotte J, Heller A, Philip BK, et al. Nmp4/CIZ suppresses parathyroid hormone-induced increases in trabecular bone. Journal of cellular physiology. Jun 2009;219(3):734–43. Epub 2009/02/04. [PubMed: 19189321]
33. Childress P, Philip BK, Robling AG, Bruzzaniti A, Kacena MA, Bivi N, et al. Nmp4/CIZ suppresses the response of bone to anabolic parathyroid hormone by regulating both osteoblasts and osteoclasts. Calcified tissue international. Jul 2011;89(1):74–89. [PubMed: 21607813]
34. He Y, Childress P, Hood M Jr., Alvarez M, Kacena MA, Hanlon M, et al. Nmp4/CIZ suppresses the parathyroid hormone anabolic window by restricting mesenchymal stem cell and osteoprogenitor frequency. Stem cells and development. Feb 1 2013;22(3):492–500. [PubMed: 22873745]
35. Childress P, Stayrook KR, Alvarez MB, Wang Z, Shao Y, Hernandez-Buquer S, et al. Genome-Wide Mapping and Interrogation of the Nmp4 Antianabolic Bone Axis. Molecular endocrinology. Sep 2015;29(9):1269–85. [PubMed: 26244796]
36. Shao Y, Hernandez-Buquer S, Childress P, Stayrook KR, Alvarez MB, Davis H, et al. Improving Combination Osteoporosis Therapy In a Preclinical Model of Heightened Osteoanabolism. Endocrinology. 2017;158(9):2722–40. [PubMed: 28637206]
37. Shao Y, Wichern E, Childress PJ, Adaway M, Misra J, Klunk A, et al. Loss of Nmp4 optimizes osteogenic metabolism and secretion to enhance bone quality. American journal of physiology Endocrinology and metabolism. May 1 2019;316(5):E749–e72. Epub 2019/01/16. [PubMed: 30645175]
38. Yang S, Adaway M, Du J, Huang S, Sun J, Bidwell JP, et al. NMP4 regulates the innate immune response to influenza A virus infection. Mucosal Immunol. Jan 2021;14(1):209–18. Epub 2020/03/11. [PubMed: 32152414]
39. Bidwell J, Tersey SA, Adaway M, Bone RN, Creecy A, Klunk A, et al. Nmp4, a Regulator of Induced Osteoanabolism, Also Influences Insulin Secretion and Sensitivity. Calcified tissue international. Feb 2022;110(2):244–59. Epub 2021/08/22. [PubMed: 34417862]
40. Thunyakitpisal P, Alvarez M, Tokunaga K, Onyia JE, Hock J, Ohashi N, et al. Cloning and functional analysis of a family of nuclear matrix transcription factors (NP/NMP4) that regulate type I collagen expression in osteoblasts. Journal of bone and mineral research : the official journal of the American Society for Bone and Mineral Research. Jan 2001;16(1):10–23. Epub 2001/01/10. [PubMed: 11149472]
41. Esen E, Lee SY, Wice BM, Long F. PTH Promotes Bone Anabolism by Stimulating Aerobic Glycolysis via IGF Signaling. Journal of bone and mineral research : the official journal of the American Society for Bone and Mineral Research. Nov 2015;30(11):1959–68. Epub 2015/05/21. [PubMed: 25990470]
42. Young SK, Shao Y, Bidwell JP, Wek RC. Nuclear Matrix Protein 4 is a Novel Regulator of Ribosome Biogenesis and Controls the Unfolded Protein Response Via Repression of Gadd34 Expression. The Journal of biological chemistry. Apr 29 2016. Epub 2016/05/01.
43. Walter P, Ron D. The unfolded protein response: from stress pathway to homeostatic regulation. Science. Nov 25 2011;334(6059):1081–6. [PubMed: 22116877]
44. Sims NA, Martin TJ. The osteoblast lineage: Its actions and communication mechanisms. Principles of Bone Biology: Elsevier; 2020. p. 89–110.
45. Creecy A, Damrath JG, Wallace JM. Control of bone matrix properties by osteocytes. Frontiers in endocrinology. 2020;11.
46. Li C, Li G, Liu M, Zhou T, Zhou H. Paracrine effect of inflammatory cytokine-activated bone marrow mesenchymal stem cells and its role in osteoblast function. Journal of bioscience and bioengineering. 2016;121(2):213–9. [PubMed: 26315505]

47. Logan M, Martin JF, Nagy A, Lobe C, Olson EN, Tabin CJ. Expression of Cre Recombinase in the developing mouse limb bud driven by a Prxl enhancer. Genesis. Jun 2002;33(2):77–80. Epub 2002/07/12. [PubMed: 12112875]
48. Zhang M, Xuan S, Bouxsein ML, von Stechow D, Akeno N, Faugere MC, et al. Osteoblast-specific knockout of the insulin-like growth factor (IGF) receptor gene reveals an essential role of IGF signaling in bone matrix mineralization. The Journal of biological chemistry. Nov 15 2002;277(46):44005–12. Epub 2002/09/07. [PubMed: 12215457]
49. Tu X, Rhee Y, Condon KW, Bivi N, Allen MR, Dwyer D, et al. Sost downregulation and local Wnt signaling are required for the osteogenic response to mechanical loading. Bone. Jan 2012;50(1):209–17. Epub 2011/11/15. [PubMed: 22075208]
50. Bivi N, Condon KW, Allen MR, Farlow N, Passeri G, Brun LR, et al. Cell autonomous requirement of connexin 43 for osteocyte survival: consequences for endocortical resorption and periosteal bone formation. Journal of bone and mineral research : the official journal of the American Society for Bone and Mineral Research. Feb 2012;27(2):374–89. Epub 2011/10/27. [PubMed: 22028311]
51. Stern AR, Stern MM, Van Dyke ME, Jähn K, Prideaux M, Bonewald LF. Isolation and culture of primary osteocytes from the long bones of skeletally mature and aged mice. BioTechniques. Jun 2012;52(6):361–73. Epub 2012/06/07. [PubMed: 22668415]
52. Han HS, Ju F, Geng S. In vivo and in vitro effects of PTH1–34 on osteogenic and adipogenic differentiation of human bone marrow-derived mesenchymal stem cells through regulating microRNA-155. Journal of cellular biochemistry. Nov 1 2017. Epub 2017/11/02.
53. Ma YL, Bryant HU, Zeng Q, Schmidt A, Hoover J, Cole HW, et al. New bone formation with teriparatide [human parathyroid hormone-(1–34)] is not retarded by long-term pretreatment with alendronate, estrogen, or raloxifene in ovariectomized rats. Endocrinology. May 2003;144(5):2008–15. Epub 2003/04/17. [PubMed: 12697709]
54. Iwamoto R, Takahashi T, Yoshimi K, Imai Y, Koide T, Hara M, et al. Chemokine ligand 28 (CCL28) negatively regulates trabecular bone mass by suppressing osteoblast and osteoclast activities. Journal of bone and mineral metabolism. Jul 2021;39(4):558–71. Epub 2021/03/16. [PubMed: 33721112]
55. Hsiao EC, Boudignon BM, Chang WC, Bencsik M, Peng J, Nguyen TD, et al. Osteoblast expression of an engineered Gs-coupled receptor dramatically increases bone mass. Proceedings of the National Academy of Sciences of the United States of America. Jan 29 2008;105(4):1209–14. Epub 2008/01/24. [PubMed: 18212126]
56. Wattanachanya L, Wang L, Millard SM, Lu WD, O'Carroll D, Hsiao EC, et al. Assessing the osteoblast transcriptome in a model of enhanced bone formation due to constitutive Gs-G protein signaling in osteoblasts. Experimental cell research. May 1 2015;333(2):289–302. Epub 2015/02/24. [PubMed: 25704759]
57. Dempster DW, Compston JE, Drezner MK, Glorieux FH, Kanis JA, Malluche H, et al. Standardized nomenclature, symbols, and units for bone histomorphometry: a 2012 update of the report of the ASBMR Histomorphometry Nomenclature Committee. Journal of bone and mineral research : the official journal of the American Society for Bone and Mineral Research. Jan 2013;28(1):2–17. Epub 2012/12/01. [PubMed: 23197339]
58. Robling AG, Kedlaya R, Ellis SN, Childress PJ, Bidwell JP, Bellido T, et al. Anabolic and catabolic regimens of human parathyroid hormone 1–34 elicit bone- and envelope-specific attenuation of skeletal effects in Sost-deficient mice. Endocrinology. Aug 2011;152(8):2963–75. [PubMed: 21652726]
59. Mizoguchi T, Ono N. The diverse origin of bone-forming osteoblasts. Journal of bone and mineral research : the official journal of the American Society for Bone and Mineral Research. Aug 2021;36(8):1432–47. Epub 2021/07/03. [PubMed: 34213032]
60. Liu Y, Strecker S, Wang L, Kronenberg MS, Wang W, Rowe DW, et al. Osterix-cre labeled progenitor cells contribute to the formation and maintenance of the bone marrow stroma. PloS one. 2013;8(8):e71318. Epub 2013/08/21. [PubMed: 23951132]
61. Mizoguchi T, Pinho S, Ahmed J, Kunisaki Y, Hanoun M, Mendelson A, et al. Osterix marks distinct waves of primitive and definitive stromal progenitors during bone marrow development. Developmental cell. May 12 2014;29(3):340–9. Epub 2014/05/16. [PubMed: 24823377]

62. Böhm AM, Dirckx N, Tower RJ, Peredo N, Vanuytven S, Theunis K, et al. Activation of Skeletal Stem and Progenitor Cells for Bone Regeneration Is Driven by PDGFRβ Signaling. Developmental cell. Oct 21 2019;51(2):236–54.e12. Epub 2019/09/24. [PubMed: 31543445]

63. Yang M, Arai A, Udagawa N, Zhao L, Nishida D, Murakami K, et al. Parathyroid Hormone Shifts Cell Fate of a Leptin Receptor-Marked Stromal Population from Adipogenic to Osteoblastic Lineage. Journal of bone and mineral research : the official journal of the American Society for Bone and Mineral Research. Oct 2019;34(10):1952–63. Epub 2019/06/08. [PubMed: 31173642]

64. Balani DH, Ono N, Kronenberg HM. Parathyroid hormone regulates fates of murine osteoblast precursors in vivo. The Journal of clinical investigation. Sep 1 2017;127(9):3327–38. Epub 2017/08/02. [PubMed: 28758904]

65. Bedi B, Li JY, Tawfeek H, Baek KH, Adams J, Vangara SS, et al. Silencing of parathyroid hormone (PTH) receptor 1 in T cells blunts the bone anabolic activity of PTH. Proceedings of the National Academy of Sciences of the United States of America. Mar 20 2012;109(12):E725–33. Epub 2012/03/07. [PubMed: 22393015]

66. Li JY, Walker LD, Tyagi AM, Adams J, Weitzmann MN, Pacifici R. The sclerostin-independent bone anabolic activity of intermittent PTH treatment is mediated by T-cell-produced Wnt10b. Journal of bone and mineral research : the official journal of the American Society for Bone and Mineral Research. Jan 2014;29(1):43–54. Epub 2013/12/21. [PubMed: 24357520]

67. Baron R, Kneissel M. WNT signaling in bone homeostasis and disease: from human mutations to treatments. Nature medicine. 2013;19(2):179–92.

68. Li J, Sarosi I, Cattley RC, Pretorius J, Asuncion F, Grisanti M, et al. Dkk1-mediated inhibition of Wnt signaling in bone results in osteopenia. Bone. 2006;39(4):754–66. [PubMed: 16730481]

69. Ajubi N, Klein-Nulend J, Nijweide P, Vrijheid-Lammers T, Alblas M, Burger E. Pulsating fluid flow increases prostaglandin production by cultured chicken osteocytes—a cytoskeleton-dependent process. Biochemical and biophysical research communications. 1996;225(1):62–8. [PubMed: 8769095]

70. Tian F, Wang Y, Bikle DD. IGF-1 signaling mediated cell-specific skeletal mechano-transduction. Journal of Orthopaedic Research®. 2018;36(2):576–83. [PubMed: 28980721]

71. Joeng KS, Lee Y-C, Lim J, Chen Y, Jiang M-M, Munivez E, et al. Osteocyte-specific WNT1 regulates osteoblast function during bone homeostasis. The Journal of clinical investigation. 2017;127(7):2678–88. [PubMed: 28628032]

72. Cao W, Helder MN, Bravenboer N, Wu G, Jin J, Ten Bruggenkate CM, et al. Is there a governing role of osteocytes in bone tissue regeneration? Current osteoporosis reports. 2020;18(5):541–50. [PubMed: 32676786]

73. Al-Maskari M, Care MA, Robinson E, Cocco M, Tooze RM, Doody GM. Site-1 protease function is essential for the generation of antibody secreting cells and reprogramming for secretory activity. Scientific reports. Sep 25 2018;8(1):14338. Epub 2018/09/27. [PubMed: 30254311]

74. Mills JC, Taghert PH. Scaling factors: transcription factors regulating subcellular domains. Bioessays. 2012;34(1):10–6. [PubMed: 22028036]

75. Dekaney CM, King S, Sheahan B, Cortes JE. Mist1 expression is required for Paneth cell maturation. Cellular and Molecular Gastroenterology and Hepatology. 2019;8(4):549–60. [PubMed: 31330316]

76. Lo H-YG, Jin RU, Sibbel G, Liu D, Karki A, Joens MS, et al. A single transcription factor is sufficient to induce and maintain secretory cell architecture. Genes & development. 2017;31(2):154–71. [PubMed: 28174210]

77. Khetchoumian K, Balsalobre A, Mayran A, Christian H, Chénard V, St-Pierre J, et al. Pituitary cell translation and secretory capacities are enhanced cell autonomously by the transcription factor Creb3l2. Nature communications. 2019;10(1):1–13.

78. Fox RM, Andrew DJ. Transcriptional regulation of secretory capacity by bZip transcription factors. Frontiers in biology. 2015;10(1):28–51. [PubMed: 25821458]

79. Capoccia BJ, Lennerz JK, Bredemeyer AJ, Klco JM, Frater JL, Mills JC. Transcription factor MIST1 in terminal differentiation of mouse and human plasma cells. Physiological genomics. 2011;43(3):174–86. [PubMed: 21098683]

80. Hess DA, Strelau KM, Karki A, Jiang M, Azevedo-Pouly AC, Lee A-H, et al. MIST1 links secretion and stress as both target and regulator of the unfolded protein response. Molecular and cellular biology. 2016;36(23):2931–44. [PubMed: 27644325]

81. Cho CJ, Park D, Mills JC. ELAPOR1 is a secretory granule maturation-promoting factor that is lost during paligenosis. American Journal of Physiology-Gastrointestinal and Liver Physiology. 2022;322(1):G49–G65. [PubMed: 34816763]

82. Huh WJ, Esen E, Geahlen JH, Bredemeyer AJ, Lee AH, Shi G, et al. XBP1 controls maturation of gastric zymogenic cells by induction of MIST1 and expansion of the rough endoplasmic reticulum. Gastroenterology. Dec 2010;139(6):2038–49. Epub 2010/09/08. [PubMed: 20816838]

83. Shaffer AL, Shapiro-Shelef M, Iwakoshi NN, Lee AH, Qian SB, Zhao H, et al. XBP1, downstream of Blimp-1, expands the secretory apparatus and other organelles, and increases protein synthesis in plasma cell differentiation. Immunity. Jul 2004;21(1):81–93. Epub 2004/09/04. [PubMed: 15345222]

84. Lee AH, Chu GC, Iwakoshi NN, Glimcher LH. XBP-1 is required for biogenesis of cellular secretory machinery of exocrine glands. The EMBO journal. Dec 21 2005;24(24):4368–80. Epub 2005/12/20. [PubMed: 16362047]

85. Hetz C, Martinon F, Rodriguez D, Glimcher LH. The unfolded protein response: integrating stress signals through the stress sensor IRE1α. Physiol Rev. Oct 2011;91(4):1219–43. Epub 2011/10/21. [PubMed: 22013210]

86. Nakamoto T, Izu Y, Kawasaki M, Notomi T, Hayata T, Noda M, et al. Mice Deficient in CIZ/NMP4 Develop an Attenuated Form of K/BxN-Serum Induced Arthritis. Journal of cellular biochemistry. Apr 2016;117(4):970–7. Epub 2015/09/18. [PubMed: 26378628]

87. Dudley HR, Spiro D. The fine structure of bone cells. The Journal of Cell Biology. 1961;11(3):627–49.

88. Schaffler MB, Cheung W-Y, Majeska R, Kennedy O. Osteocytes: master orchestrators of bone. Calcified tissue international. 2014;94(1):5–24. [PubMed: 24042263]

89. Irie K, Ejiri S, Sakakura Y, Shibui T, Yajima T. Matrix mineralization as a trigger for osteocyte maturation. Journal of Histochemistry & Cytochemistry. 2008;56(6):561–7. [PubMed: 18319272]

90. Irie K, Ozawa H, Yajima T. The histochemical and cytochemical changes from formative to resorptive osteocytes. Acta histochemica et cytochemica. 2000;33(5):385–91.

91. Piemontese M, Onal M, Xiong J, Han L, Thostenson JD, Almeida M, et al. Low bone mass and changes in the osteocyte network in mice lacking autophagy in the osteoblast lineage. Scientific reports. 2016;6(1):1–13. [PubMed: 28442746]

92. Dallas SL, Bonewald LF. Dynamics of the transition from osteoblast to osteocyte. Annals of the New York Academy of Sciences. 2010;1192(1):437–43. [PubMed: 20392270]

93. Gong Y, Yang J, Li X, Zhou C, Chen Y, Wang Z, et al. A systematic dissection of human primary osteoblasts in vivo at single-cell resolution. Aging (Albany NY). Aug 24 2021;13(16):20629–50. Epub 2021/08/25. [PubMed: 34428745]

94. Liu F, Malaval L, Aubin JE. The mature osteoblast phenotype is characterized by extensive plasticity. Experimental cell research. Apr 10 1997;232(1):97–105. Epub 1997/04/10. [PubMed: 9141626]

95. Candeliere GA, Liu F, Aubin JE. Individual osteoblasts in the developing calvaria express different gene repertoires. Bone. Apr 2001;28(4):351–61. Epub 2001/05/05. [PubMed: 11336915]

96. Bilic-Curcic I, Kronenberg M, Jiang X, Bellizzi J, Mina M, Marijanovic I, et al. Visualizing levels of osteoblast differentiation by a two-color promoter-GFP strategy: Type I collagen-GFPcyan and osteocalcin-GFPtpz. genesis. 2005;43(2):87–98. [PubMed: 16149065]

97. Manolagas SC. Birth and death of bone cells: basic regulatory mechanisms and implications for the pathogenesis and treatment of osteoporosis. Endocrine reviews. 2000;21(2):115–37. [PubMed: 10782361]

98. Jilka RL, Weinstein RS, Bellido T, Parfitt AM, Manolagas SC. Osteoblast programmed cell death (apoptosis): modulation by growth factors and cytokines. Journal of bone and mineral research. 1998;13(5):793–802. [PubMed: 9610743]

99. Hongo H, Hasegawa T, Saito M, Tsuboi K, Yamamoto T, Sasaki M, et al. Osteocytic Osteolysis in PTH-treated Wild-type and Rankl(−/−) Mice Examined by Transmission Electron

Microscopy, Atomic Force Microscopy, and Isotope Microscopy. J Histochem Cytochem. Oct 2020;68(10):651–68. Epub 2020/09/19. [PubMed: 32942927]

100. Abdelmagid SM, Belcher JY, Moussa FM, Lababidi SL, Sondag GR, Novak KM, et al. Mutation in osteoactivin decreases bone formation in vivo and osteoblast differentiation in vitro. Am J Pathol. Mar 2014;184(3):697–713. Epub 2014/01/28. [PubMed: 24462663]
101. Dallas SL, Xie Y, Shiflett LA, Ueki Y. Mouse Cre Models for the Study of Bone Diseases. Current osteoporosis reports. Aug 2018;16(4):466–77. Epub 2018/06/24. [PubMed: 29934753]
102. Zweifler LE, Koh AJ, Daignault-Newton S, McCauley LK. Anabolic actions of PTH in murine models: two decades of insights. Journal of bone and mineral research : the official journal of the American Society for Bone and Mineral Research. Oct 2021;36(10):1979–98. Epub 2021/06/09. [PubMed: 34101904]
103. Couasnay G, Frey C, Elefteriou F. Promoter Cre-Specific Genotyping Assays for Authentication of Cre-Driver Mouse Lines. JBMR Plus. Apr 2019;3(4):e10128. Epub 2019/05/03. [PubMed: 31044186]
104. Bockamp E, Maringer M, Spangenberg C, Fees S, Fraser S, Eshkind L, et al. Of mice and models: improved animal models for biomedical research. Physiol Genomics. Dec 3 2002;11(3):115–32. Epub 2002/12/05. [PubMed: 12464688]

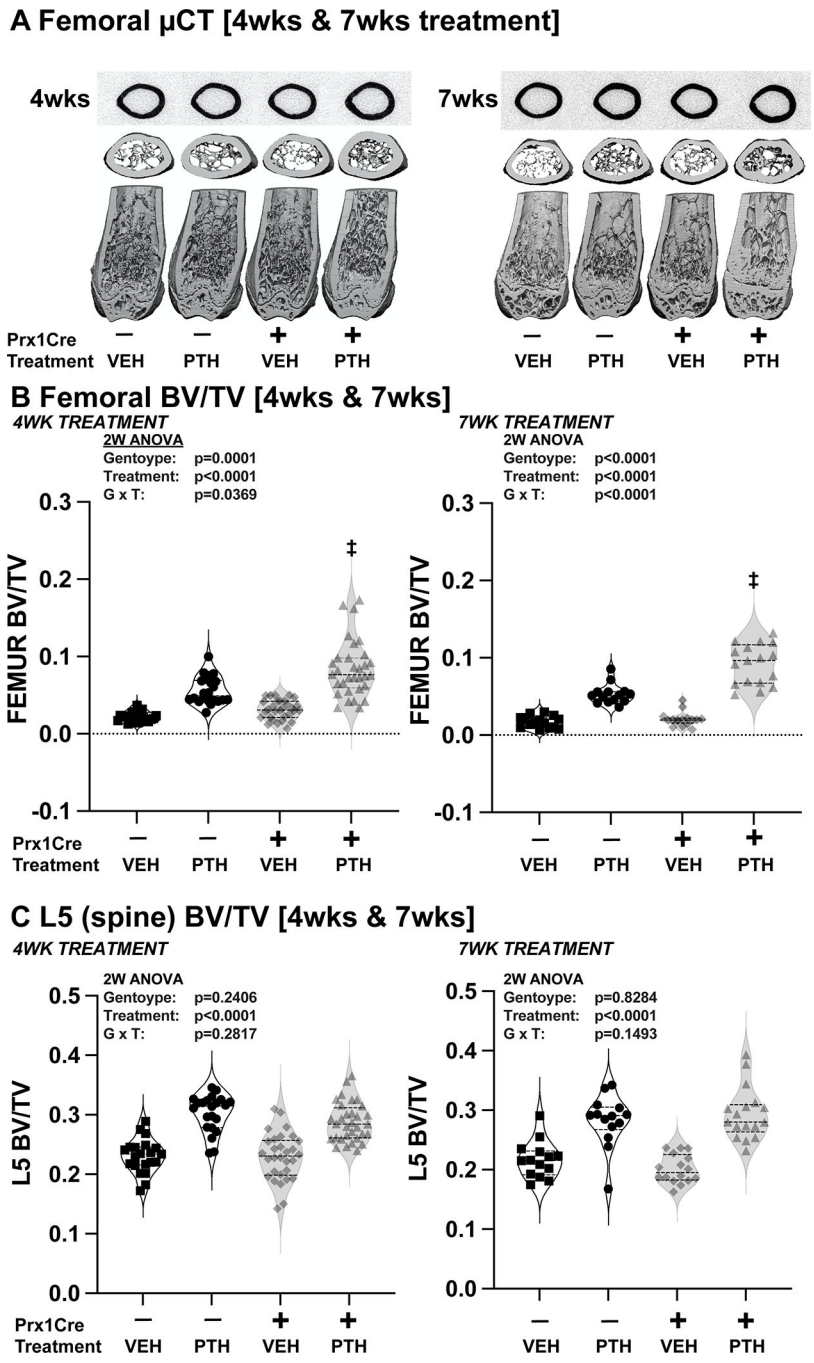

Figure 1:

Conditional loss of *Nmp4* in MSPCs enhances PTH-induced osteoanabolism. **[A]** µCT reconstructions of the distal femur from *Nmp4*$^{fl/fl}$;*Prx1Cre*− VEH, *Nmp4*$^{fl/fl}$;*Prx1Cre*− PTH, *Nmp4*$^{fl/fl}$;*Prx1Cre*+ VEH, *Nmp4*$^{fl/fl}$;*Prx1Cre*+ PTH mice at 4wks and 7wks. The images were from mice reflecting the median values of their respective cohorts. Raw data distribution and statistical analysis are shown for the **[B]** distal femoral BV/TV of the four cohorts after 4wks and 7wks of treatment and for **[C]** the lumbar L5 BV/TV of the four cohorts after 4wks and 7wks of treatment n=15–32/cohort. Data distribution is represented

using violin plots showing the median and the quartiles as dashed lines. Statistical analyses employed 2W ANOVAs using genotype and treatment as the independent variables. p-Values for individual main effects and for the interaction term are presented in each panel. ‡$p \leq 0.05$ for comparison between PTH-treated groups (testing for genotype difference among PTH-treated groups). Post hoc analyses including Student's t-test and Tukey's HSD comparisons between all cohorts are presented in Supplemental Table S1.

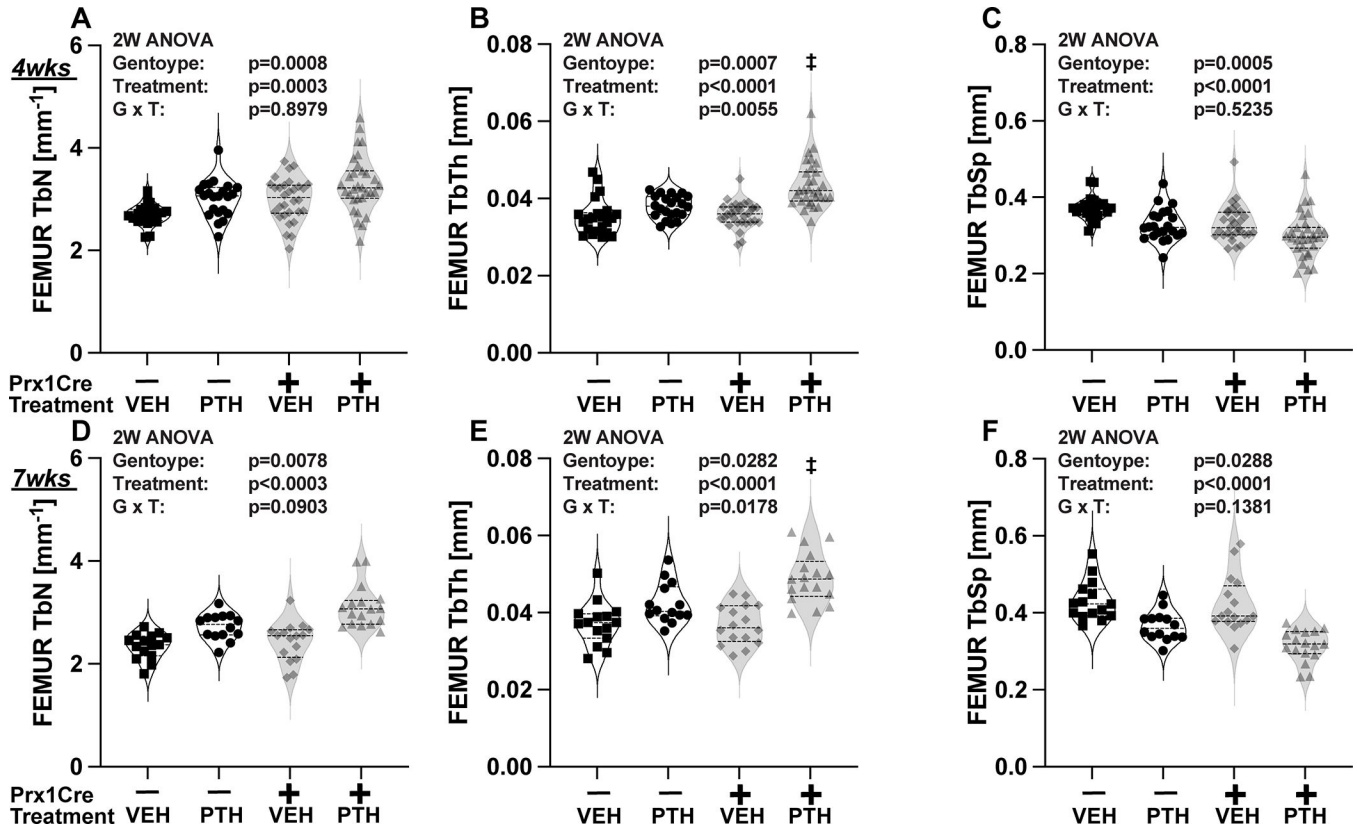

Figure 2:

Conditional loss of *Nmp4* in MSPCs enhances trabecular architecture. Raw data distribution and statistical analysis of μCT measurements of the trabecular number (TbN), trabecular thickness (TbTh), and trabecular spacing (TbSp) for the four cohorts *Nmp4*$^{fl/fl}$;*Prx1Cre*− VEH, *Nmp4*$^{fl/fl}$;*Prx1Cre*− PTH, *Nmp4*$^{fl/fl}$;*Prx1Cre*+ VEH, *Nmp4*$^{fl/fl}$;*Prx1Cre*+ PTH n = 15–32/cohort at **[A-C]** 4wks treatment and **[D-F]** 7wks treatment. PTH-induced increases in TbTh were enhanced in the *Nmp4*$^{fl/fl}$;*Prx1Cre*+ mice at both 4wks and 7wks treatment. Data distribution is represented using violin plots showing the median and the quartiles as dashed lines. Statistical analyses employed 2W ANOVAs using genotype and treatment as the independent variables. p-Values for individual main effects and for the interaction term are presented in each panel. ‡$p \leq 0.05$ for comparison between PTH-treated groups (testing for genotype difference among PTH-treated groups). Post hoc analyses including Student's t-test and Tukey's HSD comparisons between all cohorts are presented in Supplemental Table S1.

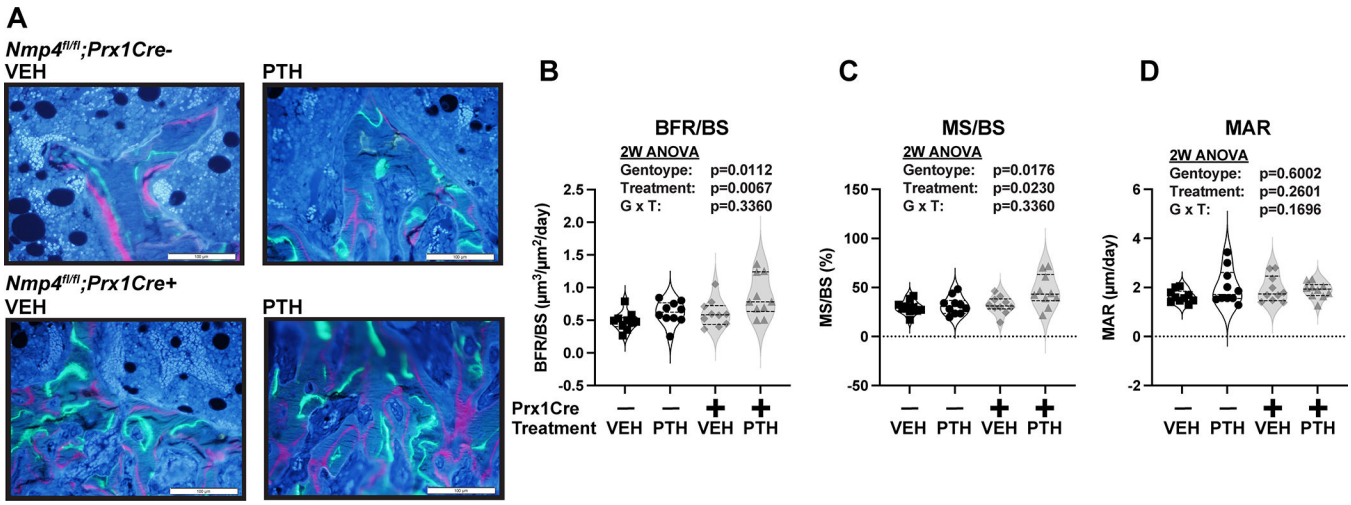

Figure 3:

Conditional loss of *Nmp4* in MSPCs enhances bone remodeling. **[A]** Representative longitudinal sections of fluorochrome-labeled (calcein green and alizarin red) femurs from the four cohorts *Nmp4*$^{fl/fl}$*;Prx1Cre*− VEH, *Nmp4*$^{fl/fl}$*;Prx1Cre*− PTH, *Nmp4*$^{fl/fl}$*;Prx1Cre*+ VEH, *Nmp4*$^{fl/fl}$*;Prx1Cre*+ PTH mice at 4wks treatment from 10wks to 14wks of age. Raw data distribution and statistical analysis are shown for **[B]** bone formation rate/bone surface (BFR/BS), **[C]** MS/BS mineralizing surface/bone surface and **[D]** MAR, matrix apposition rate (n=10/cohort). *Nmp4*$^{fl/fl}$*;Prx1Cre*+ mice had a significantly higher BFR/BS and MS/BS than their *Nmp4*$^{fl/fl}$*;Prx1Cre*− controls. Data distribution is represented using violin plots showing the median and the quartiles as dashed lines. Statistical analyses employed 2W ANOVAs using genotype and treatment as the independent variables. p-Values for individual main effects and for the interaction term are presented in each panel. Post hoc analyses are presented in Supplemental Table S1.

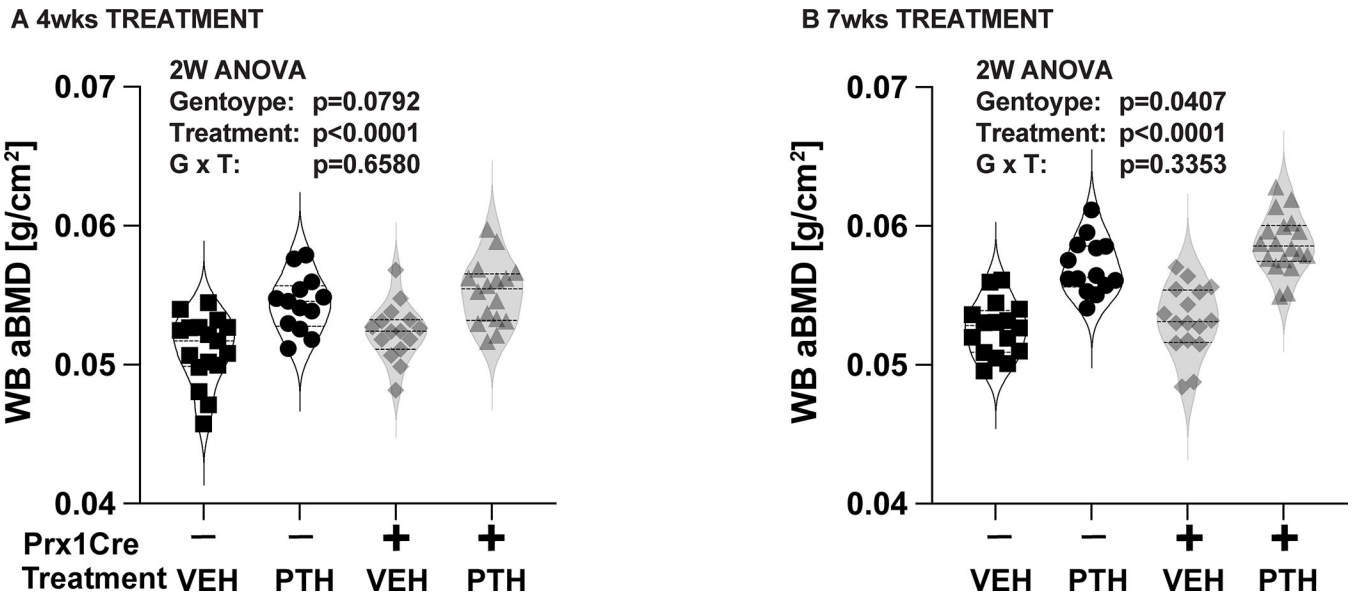

Figure 4:

Conditional loss of *Nmp4* in MSPCs enhances whole body (WB) aBMD. Raw data distribution and statistical analysis are shown for DEXA measurements of the postcranial WB aBMD from the four cohorts *Nmp4*$^{fl/fl}$;*Prx1Cre*− VEH, *Nmp4*$^{fl/fl}$;*Prx1Cre*− PTH, *Nmp4*$^{fl/fl}$;*Prx1Cre*+ VEH, *Nmp4*$^{fl/fl}$;*Prx1Cre*+ PTH at **[A]** 4wks treatment and **[B]** 7wks treatment n= 13–18/cohort. Data distribution is represented using violin plots showing the median and the quartiles as dashed lines. Statistical analyses employed 2W ANOVAs using genotype and treatment as the independent variables. p-Values for individual main effects and for the interaction term are presented in each panel. Post hoc analyses are presented in Supplemental Table S1.

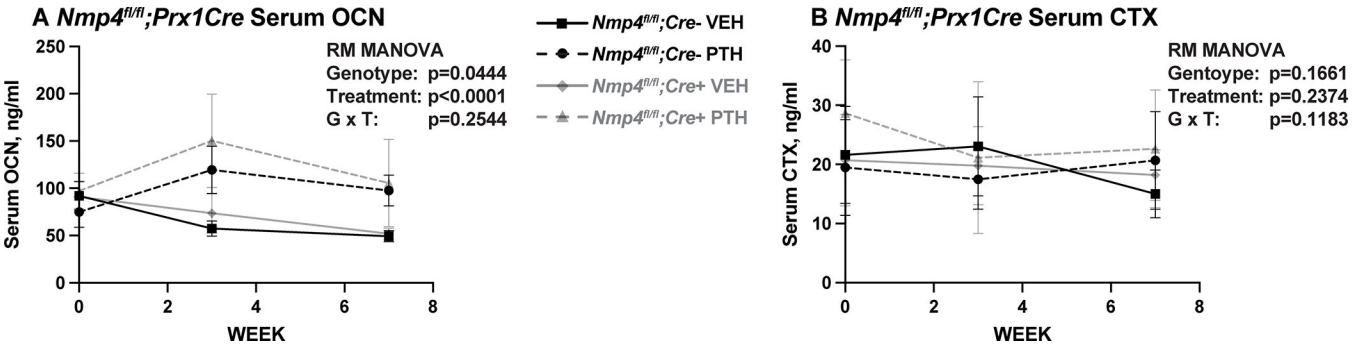

Figure 5:

Nmp4$^{fl/fl}$*;Prx1Cre*+ mice showed significantly elevated serum osteocalcin (OCN) over the 7wks PTH treatment period compared to their Cre− controls. ELISA-derived serum profiles and statistical analysis of the four cohorts *Nmp4*$^{fl/fl}$*;Prx1Cre*− VEH, *Nmp4*$^{fl/fl}$*;Prx1Cre*− PTH, *Nmp4*$^{fl/fl}$*;Prx1Cre*+ VEH, *Nmp4*$^{fl/fl}$*;Prx1Cre*+ PTH measured at 0wks (baseline), 3wks, and 7wks n=6–7/cohort for **[A]** OCN and **[B]** CTX. Data is represented using linear plots showing the average ± SD. Statistical analyses employed repeated-measures MANOVAs using genotype and treatment as the independent variables. Statistical significance was set at $p \leq 0.05$.

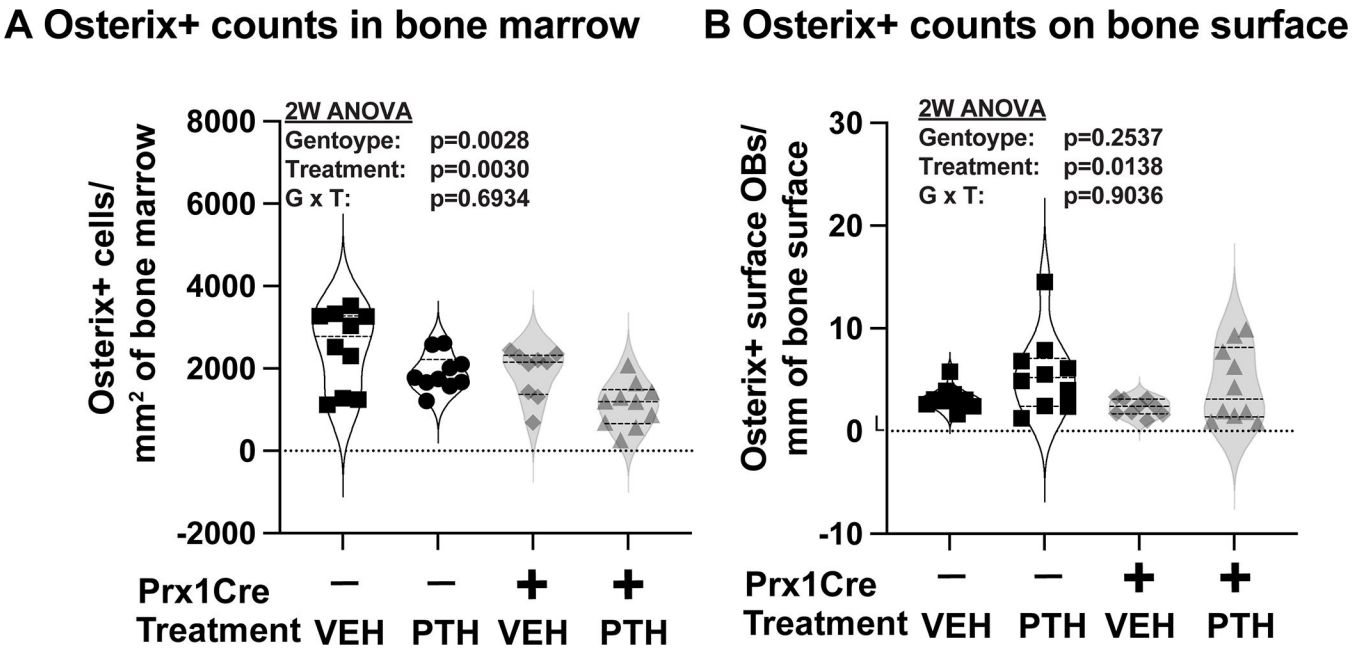

Figure 6:

Nmp4$^{fl/fl}$*;Prx1Cre*+ mice exhibited significantly lower numbers of bone marrow osterix+ cells compared to their Cre− controls. **[A]** Raw data distribution of the number of bone marrow osterix-positive cells/mm^2 in the four cohorts *Nmp4*$^{fl/fl}$*;Prx1Cre*− VEH, *Nmp4*$^{fl/fl}$*;Prx1Cre*− PTH, *Nmp4*$^{fl/fl}$*;Prx1Cre*+ VEH, *Nmp4*$^{fl/fl}$*;Prx1Cre*+ PTH mice at 7wks treatment. PTH significantly decreased the number of cells/mm^2 of both Cre+ and Cre− mice. Additionally, the *Nmp4*$^{fl/fl}$*;Prx1Cre*+ mice had significantly less osterix-positive cells than the *Nmp4*$^{fl/fl}$*;Prx1Cre*− mice. **[B]** Raw data distribution of the number of osterix-positive cells along the bone trabecular surface in the four cohorts. PTH significantly increased the number of osterix-positive cells in both genotypes. Data distribution is represented using violin plots showing the median and the quartiles as dashed lines. A single section from each mouse was used to obtain the number of osterix-positive cells and n=9–10 mice/cohort were analyzed. Statistical analyses employed 2W ANOVAs using genotype and treatment as the independent variables. p-Values for individual main effects and for the interaction term are presented in each panel. Post hoc analyses are presented in Supplemental Table S1. Representative formalin-fixed, paraffin-embedded sections of mouse bone marrow evaluated for osterix with a primary antibody from Abcam (human anti-SP7/ osterix; ab 94744; Cambridge, MA) as described in Materials and Methods and shown in Supplemental Figure S2.

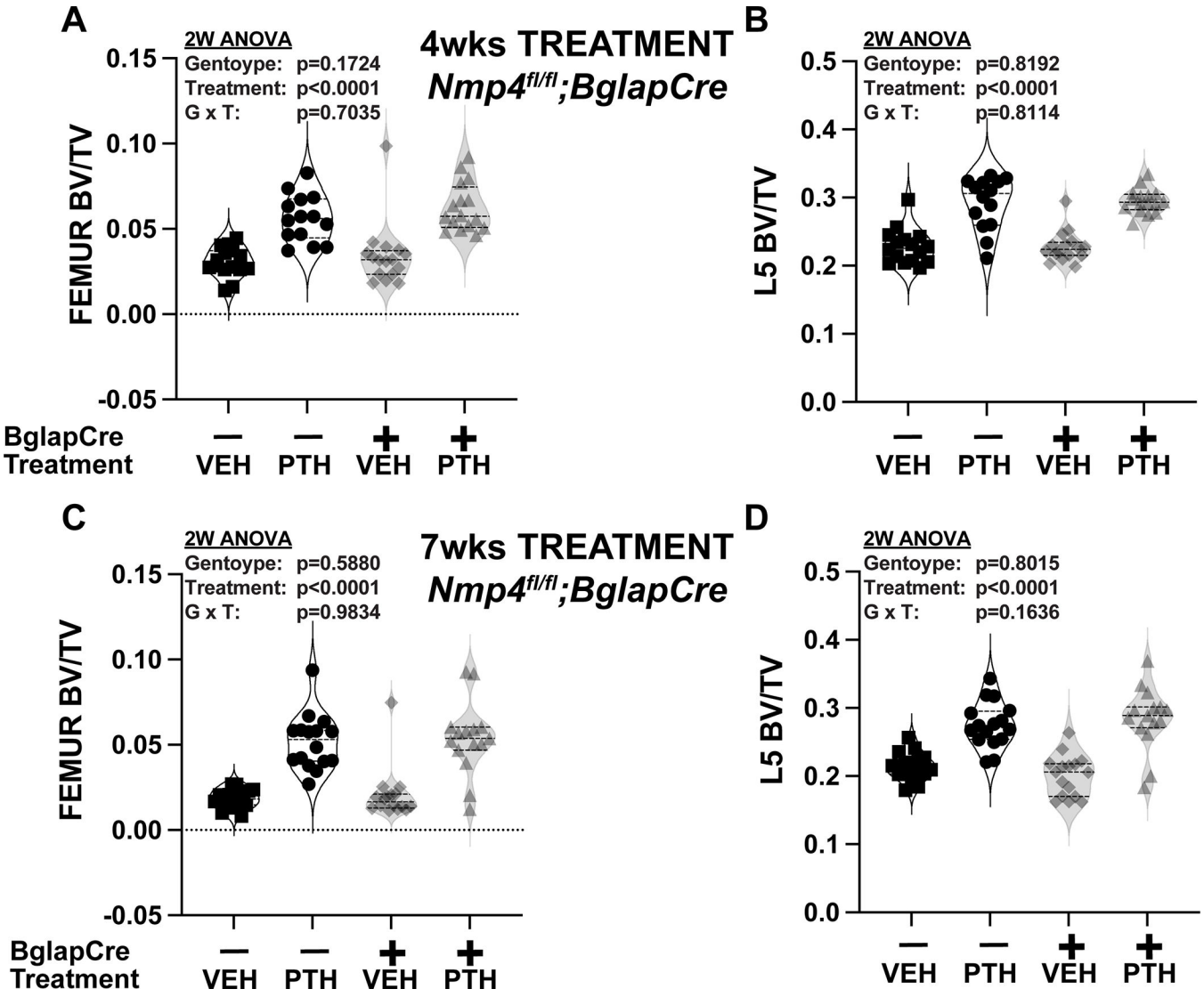

Figure 7:

Conditional loss of *Nmp4* in mature osteocalcin-expressing osteoblasts has no effect on femoral or L5 vertebra BV/TV or PTH-induced increases in these parameters. Raw data distribution and statistical analysis are shown for the distal femoral BV/TV and the L5 vertebra BV/TV from the four cohorts *Nmp4*$^{fl/fl}$*;BglapCre*– VEH, *Nmp4*$^{fl/fl}$*;BglapCre*– PTH, *Nmp4*$^{fl/fl}$*;BglapCre*+ VEH, *Nmp4*$^{fl/fl}$*;BglapCre*+ PTH n=14–17 at **[A & B]** 4wks of treatment and **[C & D]** 7wks of treatment. Data distribution is represented using violin plots showing the median and the quartiles as dashed lines. Statistical analyses employed 2W ANOVAs using genotype and treatment as the independent variables. p-Values for individual main effects and for the interaction term are presented in each panel. Post hoc analyses are presented in Supplemental Table S1.

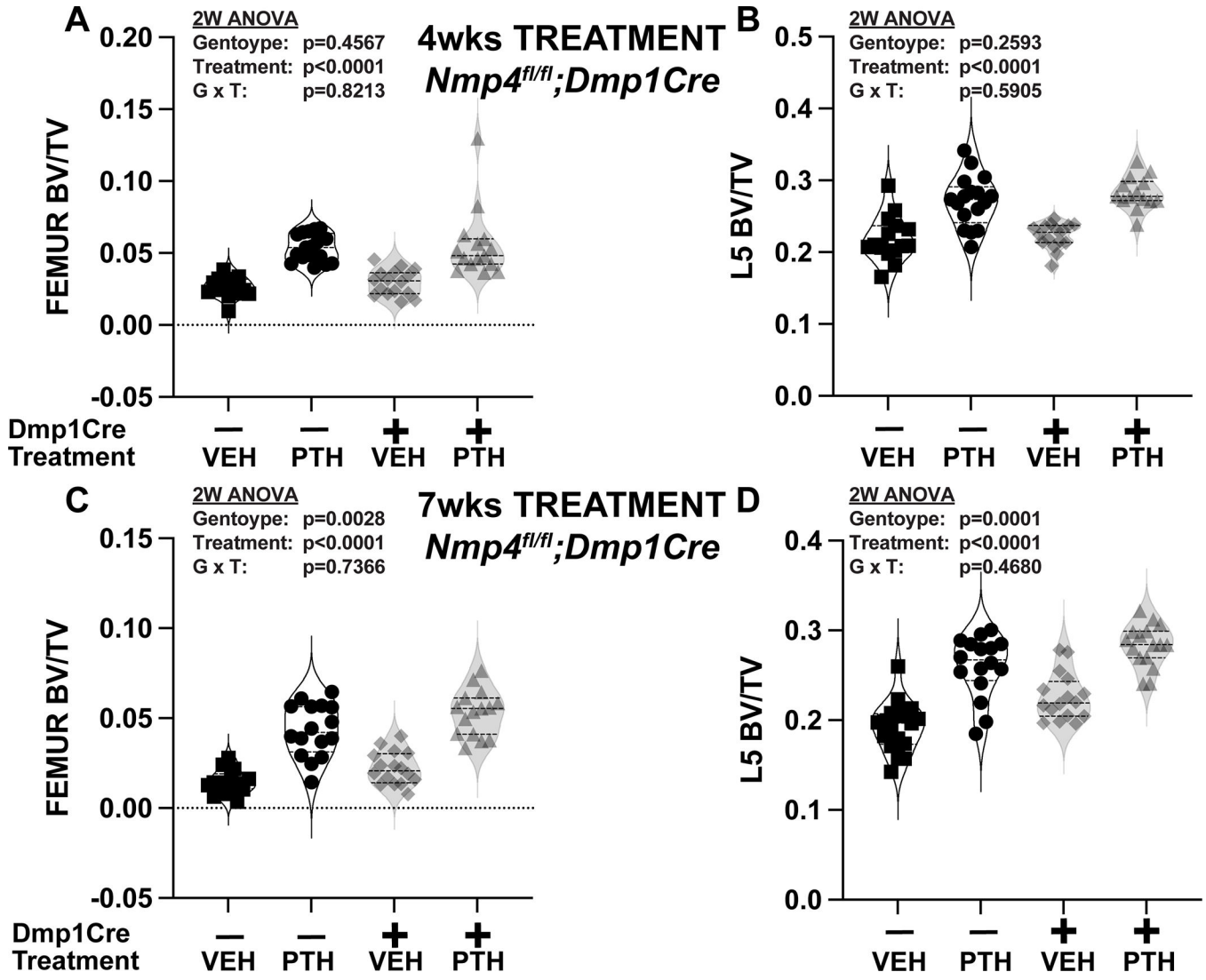

Figure 8:

Conditional loss of *Nmp4* in transitional osteocytes increases femoral and L5 vertebra BV/TV after 7wks of treatment but does not enhance the response to PTH. Raw data distribution and statistical analysis are shown for the distal femoral BV/TV and the L5 vertebra BV/TV from the four cohorts *Nmp4*$^{fl/fl}$*;Dmp1Cre*− VEH, *Nmp4*$^{fl/fl}$*;Dmp1Cre*− PTH, *Nmp4*$^{fl/fl}$*;Dmp1Cre*+ VEH, *Nmp4*$^{fl/fl}$*;Dmp1Cre*+ PTH n=15–18 at **[A & B]** 4wks of treatment and **[C & D]** 7wks of treatment. Data distribution is represented using violin plots showing the median and the quartiles as dashed lines. Statistical analyses employed 2W ANOVAs using genotype and treatment as the independent variables. p-Values for individual main effects and for the interaction term are presented in each panel. Post hoc analyses are presented in Supplemental Table S1.

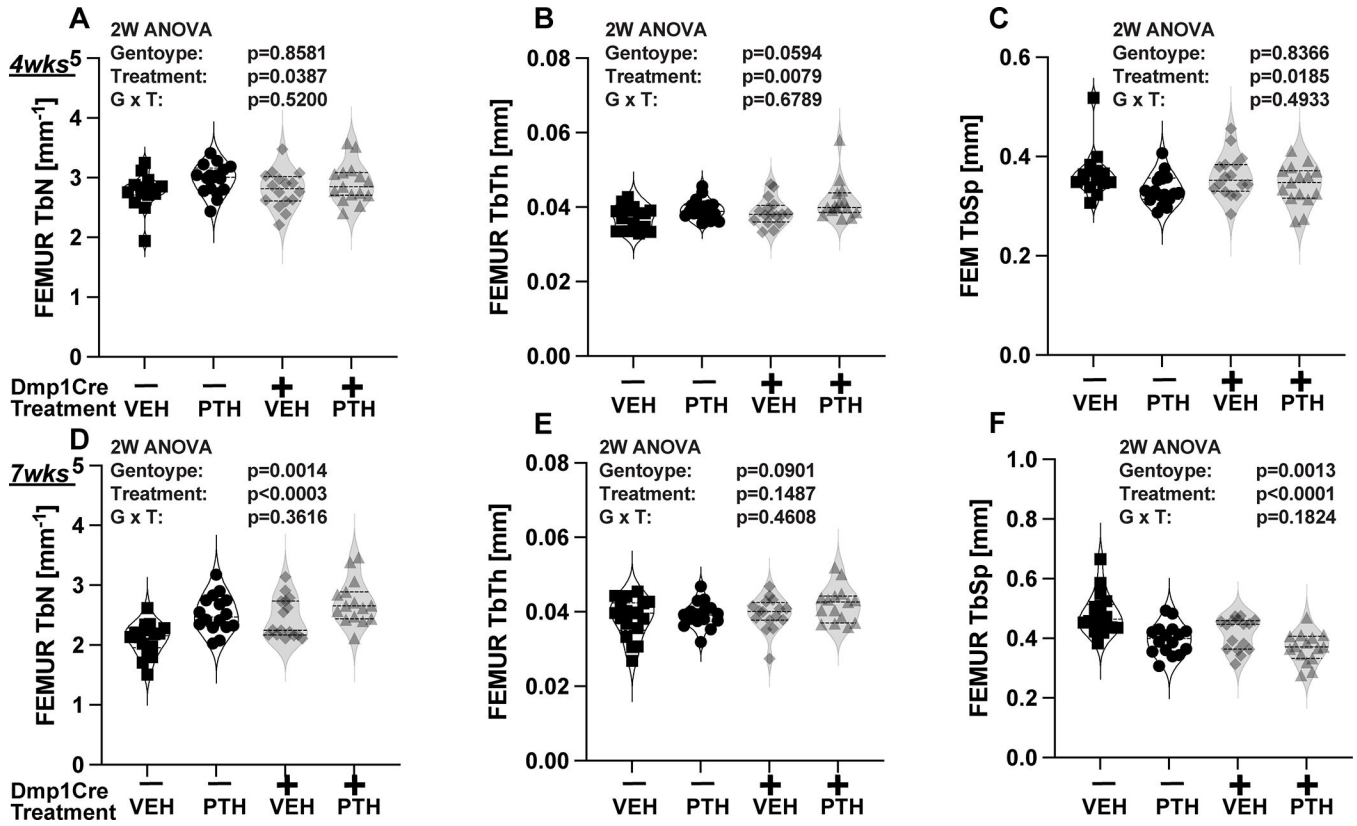

Figure 9:

Conditional loss of *Nmp4* in transitional osteocytes enhances trabecular architecture. Raw data distribution and statistical analysis of μCT measurements of the trabecular number (TbN), trabecular thickness (TbTh), and trabecular spacing (TbSp) for the four cohorts *Nmp4*$^{fl/fl}$*;Dmp1Cre*− VEH, *Nmp4*$^{fl/fl}$*;Dmp1Cre*− PTH, *Nmp4*$^{fl/fl}$*;Dmp1Cre*+ VEH, *Nmp4*$^{fl/fl}$*;Dmp1Cre*+ PTH n = 15–18/cohort at **[A-C]** 4wks treatment and **[D-F]** 7wks treatment. The *Nmp4*$^{fl/fl}$*;Dmp1Cre*+ mice showed a significantly increased TbN and decrease TbSp at 7wks. Data distribution is represented using violin plots showing the median and the quartiles as dashed lines. Statistical analyses employed 2W ANOVAs using genotype and treatment as the independent variables. p-Values for individual main effects and for the interaction term are presented in each panel. Post hoc analyses are presented in Supplemental Table S1.

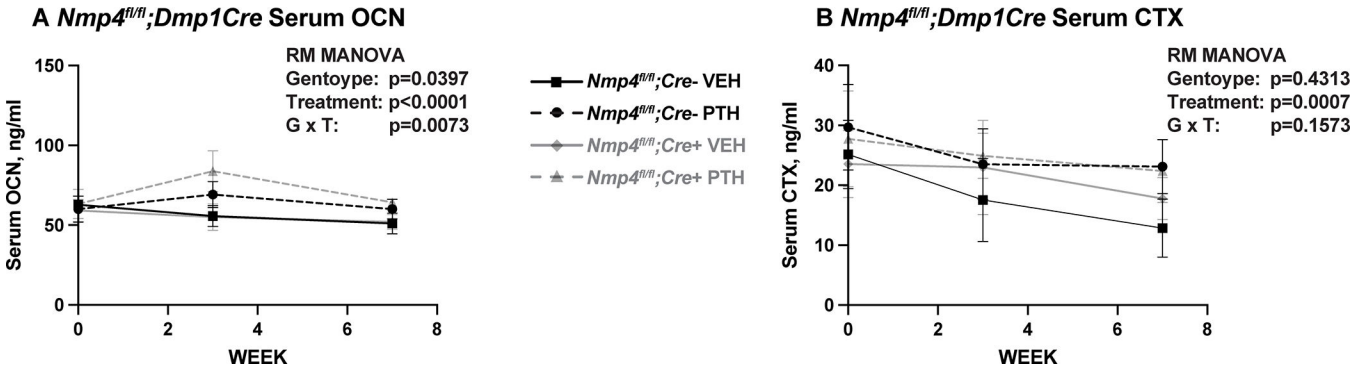

Figure 10:

Nmp4$^{fl/fl}$*;Dmp1Cre*+ mice showed significantly elevated serum osteocalcin (OCN) over the 7wks PTH treatment period compared to their Cre− controls and an enhanced response to hormone. ELISA-derived serum profiles and statistical analysis of the four cohorts *Nmp4*$^{fl/fl}$*;Dmp1Cre*− VEH, *Nmp4*$^{fl/fl}$*;Dmp1Cre*− PTH, *Nmp4*$^{fl/fl}$*;Dmp1Cre*+ VEH, *Nmp4*$^{fl/fl}$*;Dmp1Cre*+ PTH measured at 0wks (baseline), 3wks, and 7wks n=6–7/cohort for **[A]** OCN and **[B]** CTX. Data is represented using linear plots showing the average ± SD. Statistical analyses employed repeated-measures MANOVAs using genotype and treatment as the independent variables. Statistical significance was set at $p \leq 0.05$.

TABLE 1:

Nmp4$^{fl/fl}$*;Prx1Cre* mice skeletal parameters: Dual energy X-ray absorptiometry (DEXA) for areal bone mineral density and micro computed tomography (μCT) for femoral cortical parameters

		Nmp4$^{fl/fl}$*;Prx1Cre+*			*Nmp4*$^{fl/fl}$*;Prx1Cre−*		
2W ANOVA RESULTS							
DEXA aBMD g/cm^2 (7wks treatment)	**VEH**	**PTH**	**VEH**	**PTH**	**Genotype**	**Treatment**	**Genotype x Treatment**
FEMUR	0.067±0.003	0.077±0.004	0.067±0.003	0.075±0.003	p=0.0621	p<0.0001	p=0.4382
TIBIA	0.051±0.003	0.057±0.003	0.049±0.002	0.054±0.003	p=0.0013	p<0.0001	p=0.6080
SPINE (L3-L5)	0.059±0.005	0.066±0.004	0.060±0.003	0.066±0.004	p=0.6537	p<0.0001	p=0.9773
μCT Femoral cortical architecture (7wks treatment)	**VEH**	**PTH**	**VEH**	**PTH**	**Genotype**	**Treatment**	**Genotype x Treatment**
Total area mm^2	1.679±0.125	1.794±0.089	1.654±0.092	1.751±0.090	p=0.1895	p=0.0001	p=0.7344
Bone area mm^2	0.829±0.050	0.915±0.053	0.801±0.039	0.898±0.046	p=0.0752	p<0.0001	p=0.6521
Cortical Th mm	0.205±0.009	0.219±0.011	0.198±0.008	0.216±0.012	p=0.0750	p<0.0001	p=0.4250
Marrow area mm^2	0.851±0.090	0.879±0.064	0.853±0.072	0.853±0.070	p=0.5336	p=0.4747	p=0.4589
pMOI mm^4	0.344±0.046	0.399±0.040	0.331±0.034	0.383±0.038	p=0.1671	p<0.0001	p=0.8787
Imax mm^4	0.213±0.030	0.245±0.026	0.210±0.023	0.239±0.028	p=0.4961	p<0.0001	p=0.8557
Imin mm^4	0.131±0.017	0.154±0.015	0.121±0.012	0.145±0.012	p=0.0114	p<0.0001	p=0.9327

Nmp4$^{fl/fl}$*;Prx1Cre*+ and *Nmp4*$^{fl/fl}$*;Prx1Cre*− mice were treated with hPTH(1–34) (30μg/kg/d) or vehicle control from 10wks to 17wks of age. **DEXA at 7wks of treatment** showed that PTH significantly increased femur, tibial, and spine (L3-L5) aBMD (treatment p<0.0001) for both Cre+ and Cre− mice. Additionally, the *Nmp4*$^{fl/fl}$*;Prx1Cre*+ mice exhibited significantly greater WB aBMD (see Figure 5), tibial aBMD (p=0.0013) and a near significant increase in femur aBMD (p=0.0621). However, spine (L3-L5) aBMD did not significantly differ from the *Nmp4*$^{fl/fl}$*;Prx1Cre*− mice. Data represent average ± SD; n = 14–18 mice/cohort. **Femoral cortical architecture at 7wks treatment** showed there was a nearly significant genotype effect for bone area and cortical thickness revealing that these parameters trended higher in the *Nmp4*$^{fl/fl}$*;Prx1Cre*+ mice. Consistent with these results the Imin, an index of mechanical resistance to bending, was significantly higher in the *Nmp4*$^{fl/fl}$*;Prx1Cre*+ mice compared to the *Nmp4*$^{fl/fl}$*;Prx1Cre*− controls (p=0.0114). Data represent average ± SD; n = 13–17 mice/cohort. All statistical analyses were performed using two-way ANOVA tests setting genotype and treatment as the independent variables. Statistical significance was set at $p \leq 0.05$. Abbreviations: aBMD, areal bone mineral density, Cortical Th, cortical thickness; Imax, maximum moment of inertia; Imin, minimum moment of inertia; L3-L5, lumbar vertebra 3–5; pMOI, polar moment of inertia.

TABLE 2:

Nmp4$^{fl/fl}$*;BglapCre* mice skeletal parameters: Micro computed tomography (μCT) for femoral trabecular and cortical parameters; Dual energy X-ray absorptiometry (DEXA) for areal bone mineral density

		Nmp4*$^{fl/fl}$*;BglapCre+			***Nmp4*$^{fl/fl}$*;BglapCre−***		
2W ANOVA RESULTS							
μCT Femoral trabecular parameters (7wks treatment)	**VEH**	**PTH**	**VEH**	**PTH**	**Genotype**	**Treatment**	**Genotype x Treatment**
TbN (mm^{-1})	2.313±0.322	2.778±0.351	2.241±0.270	2.707±0.348	p=0.3823	p<0.0001	p=0.9925
TbTh (mm)	0.041±0.006	0.042±0.006	0.042±0.006	0.040±0.003	p=0.8531	p=0.6692	p=0.2182
TbSp (mm)	0.438±0.061	0.360±0.056	0.453±0.056	0.370±0.046	p=0.3901	p<0.0001	p=0.8664
μCT Femoral cortical parameters (7wks treatment)	**VEH**	**PTH**	**VEH**	**PTH**	**Genotype**	**Treatment**	**Genotype x Treatment**
Total area mm^2	1.692±0.085	1.824±0.085	1.632±0.076	1.729±0.108	p=0.0010	p<0.0001	p=0.4420
Bone area mm^2	0.814±0.057	0.902±0.065	0.825±0.036	0.903±0.052	p=0.6888	p<0.0001	p=0.7139
Cortical Th mm	0.198±0.011	0.213±0.017	0.206±0.008	0.220±0.014	p=0.0177	p<0.0001	p=0.8189
Marrow area mm^2	0.877±0.045	0.922±0.080	0.807±0.060	0.827±0.090	p<0.0001	p=0.0754	p=0.4863
pMOI mm^4	0.346±0.039	0.405±0.039	0.332±0.029	0.379±0.041	p=0.0345	p<0.0001	p=0.5304
Imax mm^4	0.221±0.026	0.252±0.026	0.212±0.019	0.238±0.026	p=0.0689	p<0.0001	p=0.6562
Imin mm^4	0.125±0.015	0.153±0.014	0.126±0.018	0.141±0.016	p=0.1514	p<0.0001	p=0.1411
DEXA aBMD g/cm^2 (7wks treatment)	**VEH**	**PTH**	**VEH**	**PTH**	**Genotype**	**Treatment**	**Genotype x Treatment**
WB	0.052±0.003	0.057±0.003	0.053±0.001	0.056±0.002	p=0.9772	p<0.0001	p=0.1069
FEMUR	0.067±0.005	0.074±0.004	0.068±0.002	0.073±0.004	p=0.9348	p<0.0001	p=0.1523
TIBIA	0.050±0.003	0.054±0.003	0.051±0.002	0.054±0.003	p=0.7880	p<0.0001	p=0.6121
SPINE (L3-L5)	0.059±0.005	0.067±0.005	0.060±0.004	0.065±0.004	p=0.9598	p<0.0001	p=0.0931

Nmp4$^{fl/fl}$*;BglapCre*+ and *Nmp4*$^{fl/fl}$*;BglapCre*− mice were treated with hPTH(1–34) (30μg/kg/d) or vehicle control from 10wks to 17wks of age. **Femoral trabecular bone architecture at 7wks of treatment** showed that loss of *Nmp4* in mature osteoblasts had no impact on trabecular architecture. Data represent average ± SD; n = 15–17 mice/group. **Femoral cortical architecture at 7wks treatment** showed that PTH induced significant changes in nearly all the cortical parameters in both genotypes. There were significant differences (genotype effect) in total area, cortical thickness, marrow area, and pMOI between the genotypes. Data represent average ± SD; n = 15–17 mice/group. **DEXA at 7wks of treatment** of the post-cranial skeleton (whole body, WB), femur, tibia, and spine (L3-L5) showed that PTH treatment significantly increased aBMD but there was no difference in hormone response between the two genotypes. Data represent average ± SD; n = 14–17 mice/group. All analyses were performed using two-way ANOVA setting genotype and treatment as the independent variables. Statistical significance was set at $p \leq 0.05$. Abbreviations: aBMD, areal bone mineral density; Cortical Th, cortical thickness; Imax, maximum moment of inertia; Imin, minimum moment of inertia; L3-L5, lumbar vertebra 3–5; pMOI, polar moment of inertia; TbN, trabecular number; TbTh, trabecular thickness; TbSp, trabecular space.

TABLE 3:

Nmp4$^{fl/fl}$*;Dmp1Cre* mice skeletal parameters: Femoral dynamic bone histomorphometry for remodeling, immunohistochemistry for osterix-positive cells (osteoprogenitors), dual energy X-ray absorptiometry (DEXA) for areal bone mineral density and micro computed tomography (μCT) for femoral cortical parameters

		Nmp4*$^{fl/fl}$*;Dmp1Cre+			***Nmp4*$^{fl/fl}$*;Dmp1Cre−***		
2W ANOVA RESULTS							
Femoral bone histomorphometry (4wks treatment)	**VEH**	**PTH**	**VEH**	**PTH**	**Genotype**	**Treatment**	**Genotype x Treatment**
BFR/BS μm^3/μm^2/day	0.7478±0.2626	0.8423±0.1938	0.7821±0.2003	0.7387±0.2766	p=0.6650	p=0.7497	p=0.3914
MS/BS (%)	41.75±9.57	50.28±13.15	48.58±13.60	47.21±10.72	p=0.6406	p=0.3756	p=0.2238
MAR (μm/day)	1.7520±0.3274	1.7234±0.3220	1.6432±0.2869	1.5488±0.3052	p=0.1840	p=0.5593	p=0.7546
Femoral bone immunohistochemistry (7wks treatment)	**VEH**	**PTH**	**VEH**	**PTH**	**Genotype**	**Treatment**	**Genotype x Treatment**
BM Osx+ cells/mm^2	2426±1021	1710±710	2738±740	2254±682	p=0.1009	p=0.0240	p=0.6511
Bone surface Osx+ cells/mm	2.83±1.83	3.54±1.92	2.48±1.65	4.71±3.13	p=0.5706	p=0.0460	p=0.2905
DEXA aBMD g/cm^2 (7wks treatment)	**VEH**	**PTH**	**VEH**	**PTH**	**Genotype**	**Treatment**	**Genotype x Treatment**
WB	0.053±0.002	0.057±0.002	0.053±0.002	0.056±0.002	p=0.1375	p<0.0001	p=0.7067
FEMUR	0.069±0.003	0.075±0.003	0.068±0.003	0.074±0.004	p=0.2896	p<0.0001	p=0.8534
TIBIA	0.052±0.003	0.055±0.002	0.051±0.002	0.055±0.002	p=0.6346	p<0.0001	p=0.4818
SPINE (L3-L5)	0.060±0.005	0.067±0.005	0.061±0.003	0.064±0.003	p=0.3974	p<0.0001	p=0.2012
μCT Femoral cortical architecture (7wks treatment)	**VEH**	**PTH**	**VEH**	**PTH**	**Genotype**	**Treatment**	**Genotype x Treatment**
Total area mm^2	1.676±0.085	1.811±0.121	1.655±0.087	1.774±0.073	p=0.2072	p<0.0001	p=0.7208
Bone area mm^2	0.822±0.046	0.916±0.068	0.819±0.045	0.894±0.044	p=0.3343	p<0.0001	p=0.4590
Cortical Th mm	0.202±0.009	0.217±0.013	0.202±0.009	0.214±0.011	p=0.6834	p<0.0001	p=0.5001
Marrow area mm^2	0.854±0.065	0.896±0.080	0.836±0.060	0.880±0.064	p=0.3134	p=0.0118	p=0.9433
pMOI mm^4	0.344±0.032	0.407±0.054	0.338±0.035	0.390±0.034	p=0.2349	p<0.0001	p=0.5740
Imax mm^4	0.219±0.019	0.255±0.036	0.216±0.024	0.246±0.028	p=0.3297	p<0.0001	p=0.6695
Imin mm^4	0.124±0.014	0.152±0.020	0.122±0.012	0.145±0.010	p=0.1482	p<0.0001	p=0.4517

Nmp4$^{fl/fl}$*;Dmp1Cre*+ and *Nmp4*$^{fl/fl}$*;Dmp1Cre*− mice were treated with hPTH(1–34) (30μg/kg/d) or vehicle control from 10wks to 14wks of age or from 10wks to 17wks of age. **Femoral trabecular bone histomorphometry at 4wks of treatment** show an upward trend for both BFR/BS and MS/BS in the *Nmp4*$^{fl/fl}$*;Dmp1Cre*+ mice but this was not statistically significant. Data represent average ± SD; n = 8–10 mice/group. **Femoral bone immunohistochemistry at 7wks of treatment** of osterix+ cells 1mm below the growth plate. PTH decreased the frequency of these cells in the BM but increased the number of these cells along the bone surface as the anabolic window closes. Data represent average ± SD; n = 9–10 mice/group (see Supplemental Figure 2S for examples of osterix staining. **DEXA at 7wks of treatment** of the post-cranial skeleton (whole body, WB), femur, tibia, and spine (L3-L5) showed that PTH treatment significantly increased aBMD but there was no difference in hormone response between the two genotypes. Data represent average ± SD; n = 15–16 mice/group. Femoral cortical architecture at 7wks treatment show that PTH significantly altered several parameters in both genotypes. Data represent average ± SD; n = 15–18 mice/group. Statistical analyses were performed using two-way ANOVA tests setting genotype and treatment as the independent variables. Statistical significance was set at $p \leq 0.05$. Abbreviations: aBMD, areal bone mineral density; BM, bone marrow, BFR/BS, bone formation rate/bone surface; Cortical Th, cortical

thickness; Imax, maximum moment of inertia; Imin, minimum moment of inertia; L3-L5, lumbar vertebra 3–5; MAR, matrix apposition rate; MS/BS, mineralizing surface/bone surface; pMOI, polar moment of inertia.